DEPARTMENT OF INTERNATIONAL AND EUROPEAN ECONOMIC STUDIES

ATHENS UNIVERSITY OF ECONOMICS AND BUSINESS

Climate Policy under Cooperation and Competition between Regions with Spatial Heat Transport

Yongyang Cai

William Brock

Anastasios Xepapadeas

Kenneth Judd

Working Paper Series

18-06

March 2018

Climate Policy under Cooperation and Competition between Regions with Spatial Heat Transport*

Yongyang Cai† William Brock‡ Anastasios Xepapadeas§ Kenneth Judd¶

March 26, 2018

Abstract

We build a novel stochastic dynamic regional integrated assessment model (IAM) of the climate and economic system including a number of important climate science elements that are missing in most IAMs. These elements are spatial heat transport from the Equator to the Poles, sea level rise, permafrost thaw and tipping points. We study optimal policies under cooperation and various degrees of competition between

*Cai and Brock acknowledge support from the National Science Foundation grant SES-1463644 under the auspices of the RDCEP project at the University of Chicago. Cai would also like to acknowledge support from the Hoover Institution at Stanford University. This research is part of the Blue Waters sustained-petascale computing project, which is supported by the National Science Foundation (awards OCI-0725070 and ACI-1238993) and the State of Illinois. Blue Waters is a joint effort of the University of Illinois at Urbana-Champaign and its National Center for Supercomputing Applications. A preliminary version of this paper was circulated with the title "Climate Change Economics and Heat Transport across the Globe: Spatial-DSICE".

†The Ohio State University. cai.619@osu.edu

‡University of Wisconsin and University of Missouri. wbrock@ssc.wisc.edu

§Athens University of Economics and Business and University of Bologna. xepapad@aueb.gr

¶Hoover Institution. kennethjudd@mac.com

regions. Our results suggest that when the elements of climate science which are accounted for in this paper are ignored, important policy variables such as the social cost of carbon and adaptation could be seriously biased.

Keywords: Integrated Assessment Model, spatial heat transport, social cost of carbon, carbon taxes, adaptation, sea level rise, permafrost, stochastic tipping points, Epstein-Zin preferences

JEL Classification: Q54, Q58, C61, C63

1 Introduction

A major characteristic of leading integrated assessment models (IAMs) such as RICE-2010 (Nordhaus, 2010) or DICE-2016 (Nordhaus, 2017) is that the geophysical sector of the model determines the mean surface temperature through the carbon cycle, which in turn determines the damage function. Thus damages are related to the mean surface temperature of the planet.

A well-established fact in the science of climate change, however, is that when the climate cools or warms, high latitude regions tend to exaggerate the changes seen at lower latitudes (e.g., Langen and Alexeev, 2007; IPCC, 2013). This effect is called polar amplification (PA) and indicates that, under global warming, the temperature at the latitudes closer to the Poles will increase faster than at latitudes nearer to the Equator. PA is especially strong in the Arctic and is sometimes called "Arctic amplification". For example, Bekryaev, Polyakov, and Alexeev (2010) document a high-latitude (greater than 60 °N) warming rate of 1.36 degrees centigrade per century from 1875 to 2008. This trend is almost twice that of the Northern Hemisphere trend of 0.79 degrees centigrade per century.

Spatial heat and moisture transport, and the resulting PA, suggest that a better representation of the climate science underlying IAMs would be a geophysical sector structure which accounts for these phenomena. This implies that, in the IAM output, the surface temperature anomaly will be differentiated across spatial zones of the globe. The spatial temperature differentiation

is important for the economics of climate change because it provides the impact of PA on the structure of the economic damages. PA will accelerate the loss of Arctic sea ice, which in turn has consequences for melting land ice that is associated with a potential meltdown of the Greenland and West Antarctica ice sheets which could cause serious global sea level rise (SLR).

Another source of damage associated with PA relates to the thawing of the permafrost, which is expected to bring about widespread changes in ecosystems and damage to infrastructure, along with release of greenhouse gases (GHGs) which exist in permafrost carbon stocks (see, e.g., IPCC, 2013; Schuur et al., 2015). Furthermore, recent studies suggest that Arctic amplification might increase the frequency of extreme weather events (Cohen, Pfeiffer, and Francis, 2018), although this remains a controversial issue (Overland and Wang, 2018).

The well-known "burning embers" diagram in Lenton and Schellnhuber (2007) shows the ranking of tipping elements by order of proximity to the present time. The "nearest" three potential tipping points are located in the high latitudes of the Northern Hemisphere (Arctic summer sea ice loss, Greenland ice sheet melt and boreal forest loss). Because of PA in the Arctic, each degree increase in planetary yearly mean temperature leads to approximately two degrees increase in the Arctic latitudes. Thus natural phenomena occurring in high latitudes, due to spatial heat and moisture transport, can cause economic damages in lower latitudes. These spatial impacts, which could have important implications for climate change policies, are not embodied in the current generation of IAMs. The RICE model (Nordhaus, 2010) – the regional version of DICE (Nordhaus, 2017) – still treats the climate system by using the globally averaged measure of temperature and neglects heat and moisture transport and especially PA.

Hassler and Krusell (2012) extend Golosov et al. (2014) to multi-regions. While their work is elegant, as is that of Golosov et al. (2014), they do not deal with poleward heat transport, multi-layer carbon cycles, separation of atmospheric and oceanic layers, and regional tipping points, as we do here. van der Ploeg and de Zeeuw (2016) develop an interesting two-region model with tipping points that deals explicitly with non-cooperative and cooperative

institutional structures. While their model is richer than ours in the comparison of institutional structures, they do not include poleward heat transport, recursive preferences, and the more realistic multi-layer modeling of the carbon cycle and the temperature response to anthropogenic forcing as we have. Thus neither they nor Golosov et al. (2014) and Hassler and Krusell (2012) are able to produce "fan charts" of uncertainty growth over time and effects of different values of the intertemporal elasticity of substitution (IES) and risk aversion parameters as we are able to do. They are also not able to study the effects of neglecting poleward heat transport on regional social cost of carbon (SCC) as we are able to do with our richer and more realistic modeling of the interaction between climate dynamics and economic dynamics.

Another very recent IAM model of Krusell and Smith (2017) deals with space at a much finer scale than the present paper and contrasts market structures, including autarky and full borrowing and lending. However, their model does not address issues related to heat and moisture transport, SLR, permafrost thaw and the impacts of tipping points, as we do here. Thus we feel that our work is complementary to that of Krusell and Smith (2017) and not competitive. As mentioned above, one novel contribution of the present paper is to develop an IAM which incorporates spatial impacts associated with heat and moisture transport, along with treatment of uncertainty and tipping points. As far as we know, no other IAM treats these issues as we do here.

The stochastic IAM developed in this paper is a complex two-regional model with a more realistic – relative to existing models – geophysical sector and its solution requires the use of advanced numerical methods. Thus we adapt computational methods related to the DSICE model of Cai, Judd, and Lontzek (2015). The DSICE framework is a stochastic generalization of DICE, which does not take into account the heat and moisture transport dynamics of the climate system. We adapt DSICE by disaggregating the globe into regions and incorporating Negishi weights (Negishi, 1972), which implement competitive equilibrium by respecting initial endowments, in order to solve the dynamic stochastic problems with various degrees of competition between regions in our model. Since our model is dynamic, its Negishi weights are also

time-variant and are solved numerically with an iterative method.

This approach enables us to produce fan charts which quantify the effects of realistic parameter and modeling uncertainties on key endogenous variables and show how these uncertainties grow over future projections. In particular we quantify the impact of heat and moisture transport upon these fan charts, produce distributions of the SCC, and quantify the importance on SCC distributions of adding heat and moisture transport. In this way, the impacts of realistic uncertainties on the SCC may be properly assessed. We stress that policy analysis must take into account higher moments of the uncertainty distribution of the SCC – and not just the mean – because most of the serious damages are due to higher moments. To put it another way, the SCC must be treated as a stochastic process in order to properly assess the uncertainty in the SCC which is required for risk and uncertainty management, and this treatment is accomplished in this paper.

We call our model a Dynamic Integration of Regional Economy and Spatial Climate under Uncertainty (DIRESCU).[1] In comparing the predictions of the standard DICE with the predictions of DIRESCU, using the same economic parameters, our purpose is to explore the impacts on the design of climate policy of ignoring the existing spatial transport phenomena and the associated feedbacks. An important policy relevant question is whether – by ignoring spatial transport – we overestimate or underestimate optimal emission paths, the SCC, and what the impact on the general shape of the uncertainty bands around these paths is when heat and moisture transport are neglected. In developing DIRESCU, we follow the two-region approach of Langen and Alexeev (2007) but change their regions as follows: region 1 is the region north of latitude 30°N to 90°N (called the North), while region 2 is the region from latitude 90°S (the South Pole) to 30°N (called the Tropic-South). Heat and moisture transport take place northbound from the tropical belt of latitudes north of

[1] Brock and Xepapadeas (2017) considered a simple deterministic model and showed that, by ignoring spatial heat and moisture transport and the resulting PA, the regulator may overestimate or underestimate the tax on GHG emissions. The structure of their economic model is, however, simplified and this makes it difficult to discuss realistic policy options.

the Equator which are included in the Tropic-South toward the North.[2]

The interaction of the geophysical sector of DIRESCU with the economic sector is reflected in the damage function. We introduce separate damage functions in each region and allow for damages in the Tropic-South to be caused by an increase in temperature (i.e., PA) in the North. For example, the increased amplification of the temperature anomaly in the high north latitudes increases the hazard rate of tipping events in the high north latitudes toward earlier arrival times. Hence any associated damages caused to lower latitudes by warming in the higher north latitudes, e.g., increased melting of land ice leading to SLR damages in the lower latitudes, will be increased by PA, even though the high northern latitudes may benefit from additional warming.

The rest of the economic module is based on a two-region differentiation of DICE-2016 (Nordhaus, 2017). We model the economic interactions between the regions with an adjustment cost function, and we allow for adaptation expenses in each region. Krusell and Smith (2017) compare the two market structures of complete autarky and full international borrowing and lending and find that the market structures do not have a large impact on their results. While we can study autarky as Krusell and Smith (2017) do by raising the cost of interaction to induce autarky, our formulation of economic interactions does not include the case of full borrowing and lending as in their model. We have ignored serious modeling of market structure in order to focus on elements of geophysics that are ignored in other contributions, including that of Krusell and Smith (2017), so that we may provide new insights regarding

[2]There is transport toward the South Pole from all latitudes south of the Equator in the Tropic-South which we do not take into account in order to ease the computational burden by reducing the number of dimensions in our model and at the same time include the Southern Hemisphere economies. Scientific evidence suggests that PA in Antarctica is weaker than in the Arctic, because of weaker surface albedo feedback and more efficient ocean uptake in the Southern Ocean, in combination with Antarctic ozone depletion.

Thus, for the time horizon of 100 years in which our solutions are focused, the majority of the effects of heat transfer should be associated with heat transfer toward the North Pole. In view of the above, and aiming at reducing the dimensionality of the model while incorporating the Southern Hemisphere economies, we adopted the approximation of unifying the Southern Hemisphere with the 0°-30°N belt and northbound heat transfer. Future research with more computational resources will explore whether this approximation matters.

the importance of spatial phenomena in climate change policy.

The present paper innovates relative to popular IAMs at the tractable level of complexity in the literature (e.g., Nordhaus's DICE and RICE models, the even more complex DSICE model and many others) in a number of ways and in particular by: (i) incorporating an endogenous SLR module, an endogenous permafrost melt module and, especially, adding the more realistic geophysics of spatial heat and moisture transport from low latitudes to high latitudes, while keeping the three-layer carbon cycle and two-layer temperature module of DICE and RICE; (ii) introducing recursive preferences and considering a wide range of parameter values of risk aversion and IES; (iii) going beyond the single-region DSICE model by adding a set of regional welfare weights ranging from egalitarian (equal weighting) to Negishi weights; (iv) adding a parameterization of cross border frictions ranging from autarky (very high cross border frictions) to low cross border frictions; and finally (v) allowing for adaptation to regional damage from SLR and temperature increase.[3]

We calibrate our many parameter values to match history as well as to fit the representative concentration pathway (RCP) scenarios (Meinshausen et al., 2011). The main results of this paper are summarized below.

First, regional SCC stochastic processes are derived and various uncertainty fan charts with and without tipping points are presented and compared with and without heat and moisture transport as well as for a range of risk aversion, IESs and welfare weights. Our figures and tables provide a much more thorough quantification of the multitude of types of uncertainties than the received regional IAM literature at the DICE/RICE level of complexity.

Second, neglecting heat and moisture transport as in RICE and other re-

[3]The importance of relating damages from temperature increase to adaptation has been emphasized by, for example, Barreca et al. (2016) who showed remarkable reduction of damages to morbidity and mortality due to heat stress in the U.S. after the introduction of technologies such as air conditioning. Another example is Burgess et al. (2014) who showed large negative effects of extreme heat days in India, especially in rural areas. Since lack of access to air conditioning is a difference between India and the U.S., these results suggest that because many areas in the Tropic-South are poorer than the North, we might expect adaptation such as introduction of air conditioning to be slower in the Tropic-South than in the wealthier parts of the North.

gional IAMs that do not account for this added geophysics leads to many biases, including inaccurate forecasting of the first time of arrival of potential tipping points located in the high latitudes of the Northern Hemisphere. The low (high) latitude regions would be hotter (colder) if poleward heat transport were absent, hence damages in the low latitude regions would be higher, since they are already under heat stress and transporting some of that heat poleward helps relieve this heat stress. For example, solutions without heat transport will underestimate what actual heat-related damage there is in the North, and overestimate the actual heat-related damage in the Tropic-South. Without heat transport, the adaptation rates in the North will be underestimated as its corresponding atmospheric temperature anomaly is underestimated, and the adaptation rates in the Tropic-South will be overestimated as its corresponding atmospheric temperature anomaly is overestimated.

Third, endogenous SLR is an important new contribution of our modeling. In this way we capture the projected increased diversion into adapting to SLR (e.g., spending resources on SLR-protective infrastructure). The projected earlier arrival of increased melting of land ice in the Northern Hemisphere high latitudes due to our inclusion of heat transport means a potential increase in SLR damages in coastal low latitude areas relative to the projections when heat transport is ignored.

Fourth, when welfare weights are more egalitarian, the SCC of the North increases relative to the Tropic-South and investments from the North to the Tropic-South are larger compared to the non-egalitarian Negishi weights case (i.e., competitive equilibrium).

Fifth, SCCs for both regions tend to be larger for larger IES values for climate tipping risks. This is consistent with empirical findings in finance that greater IESs in Epstein–Zin recursive preferences (Epstein and Zin, 1989) imply that long-term risk matters and SCCs are larger.[4] This result is also consistent with the findings in the DSICE model (Cai, Judd, and Lontzek, 2015).

[4]See Bansal and Yaron (2004) for financial risks, and Bansal, Kiku, and Ochoa (2016) for climate risks.

Optimal SCC paths for both regions from ignoring heat transport are higher than those with heat transport in the deterministic model. However, if we allow for stochastic tipping points, ignoring PA leads to underestimation of the SCC in both regions. This result can be regarded as supporting the case for taking action regarding climate change now rather than later. It also indicates that our approach addresses issues related to the inability of most IAMs to formulate policies when catastrophic events may arrive.

The paper is organized as follows. Section 2 builds a deterministic version of DIRESCU. We calibrate our spatial climate system and the economic system using DICE and RICE, as well as data from other literature such as IPCC (2013). Section 3 analyzes results of the deterministic version of DIRESCU. Section 4 extends the deterministic model to a stochastic one, using a tipping point as one representative risk and Epstein–Zin preferences to address the smoothness of consumption across time and risk aversion following DSICE. Section 5 discusses the results of the DIRESCU model and Section 6 concludes.

2 Deterministic Model

Our deterministic model follows DICE-2016 (Nordhaus, 2017), which maximizes social welfare with trade-offs between carbon dioxide (CO_2) abatement, consumption and investment. Our model has been augmented with an additional control, relative to DICE-2016, by including adaptation to climate change following de Bruin et al. (2009). DIRESCU has two regions: the first one (indexed with $i = 1$) is the North from latitude 30°N to 90°N and the second one (indexed with $i = 2$) is the Tropic-South from latitude 90°S to 30°N. We model it as a social planner problem with both economic and climate interaction between two regions, SLR, permafrost thaw and climate tipping risks (in the deterministic model, the risks are ignored). The big picture of the model setup is depicted in Figure 1 and its details are described below.

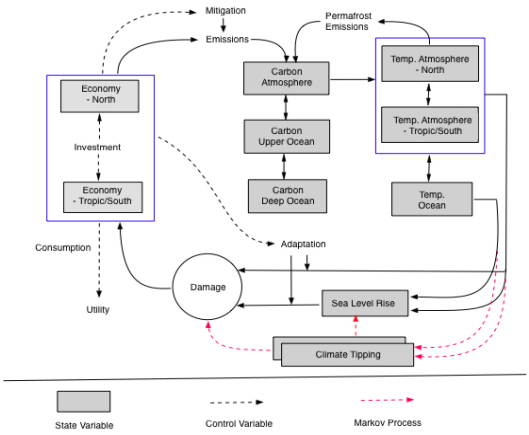

Figure 1: The DIRESCU model

2.1 The Climate System

The climate system contains four modules: the carbon cycle, the temperature system, SLR and permafrost thaw. In our calibration of the climate system, we use the four RCP scenarios (i.e., RCP2.6, RCP4.5, RCP6, and RCP8.5) (Meinshausen et al., 2011) and DICE/RICE optimal scenarios (i.e., the optimal solutions of DICE-2016 and RICE-2010 with optimal mitigation policy), where we define each scenario as a combination of pathways of global emissions, atmospheric carbon concentration, global radiative forcing, and globally averaged surface temperature relative to 1900 levels. For the RCP scenarios, the pathways of atmospheric carbon concentration, global radiative forcing, and globally averaged surface temperature are generated from the software MAGICC (Meinshausen, Raper, and Wigley, 2011), using the corresponding pathways of global emissions as the input to the software. The pathways of global emissions are provided by MAGICC too. Appendix A.2 shows that our calibrated system fits these scenarios, history, as well as other data in the literature such as regional temperature projections reported in IPCC (2013).

2.1.1 Carbon Cycle

We follow DICE-2016 in using three-layer carbon concentrations: atmospheric carbon, carbon in the upper ocean and carbon in the deep ocean. Let $\mathbf{M}_t =$

$(M_t^{\mathrm{AT}}, M_t^{\mathrm{UO}}, M_t^{\mathrm{DO}})^\top$ represent the carbon concentration in the atmosphere, the upper ocean and the deep ocean. Then the three-layer carbon cycle system can be represented as:

$$\mathbf{M}_{t+1} = \mathbf{\Phi}_{\mathrm{M}} \mathbf{M}_t + (E_t, 0, 0)^\top, \tag{1}$$

where E_t is global carbon emissions (billions of metric tons) and

$$\mathbf{\Phi}_{\mathrm{M}} = \begin{bmatrix} 1-\phi_{12} & \phi_{21} & \\ \phi_{12} & 1-\phi_{21}-\phi_{32} & \phi_{32} \\ & \phi_{23} & 1-\phi_{32} \end{bmatrix}. \tag{2}$$

The parameters ϕ_{ij} are calibrated against the four RCP scenarios and the DICE-2016 optimal scenario. For every scenario, we can use its pathway of emissions as the input E_t to our carbon cycle system (1). Our carbon cycle provides as output a pathway of atmospheric carbon concentration for each scenario. We calibrate a unique set of values for ϕ_{ij} so that the pathways of atmospheric carbon concentration are close to the scenarios' pathways of atmospheric carbon concentration, for all scenarios.

2.1.2 Temperature Subsystem

The global radiative forcing representing the impact of CO_2 concentrations on the surface temperature of the globe (watts per square meter from 1900) is

$$F_t = \eta \log_2 \left(M_t^{\mathrm{AT}} / M_*^{\mathrm{AT}} \right) + F_t^{\mathrm{EX}}, \tag{3}$$

where $\eta = 3.68$ as in DICE-2016 and F_t^{EX} is the global exogenous radiative forcing.

We use $\mathbf{T}_t = (T_{t,1}^{\mathrm{AT}}, T_{t,2}^{\mathrm{AT}}, T_t^{\mathrm{OC}})^\top$ to represent the temperature anomaly (relative to 1900 levels) in the atmosphere (two regions) and the global ocean. Thus, the temperature system is

$$\mathbf{T}_{t+1} = \mathbf{\Phi}_{\mathrm{T}} \mathbf{T}_t + \xi_1 \left(F_t, F_t, 0 \right)^\top, \tag{4}$$

where we assume that the global radiative forcing has the same effect on both regions, and

$$\mathbf{\Phi}_{\mathrm{T}} = \begin{bmatrix} 1-\xi_2-\xi_4-\xi_6 & \xi_4+\xi_5 & \xi_2 \\ \xi_4 & 1-\xi_2-\xi_4-\xi_5-\xi_6 & \xi_2 \\ \xi_3 & \xi_3 & 1-2\xi_3 \end{bmatrix}.$$

In transition equation (4) and transition matrix $\mathbf{\Phi}_{\mathrm{T}}$, the parameter ξ_1 is the temperature increase for each unit of radiative forcing, ξ_2 and ξ_3 represent transport between atmosphere and ocean, ξ_4 and ξ_5 are used to capture spatial heat and moisture transport, and ξ_6 represents the sensitivity of the outgoing long-wave radiation to atmospheric temperature changes.

Similarly to the calibration of the carbon cycle, we calibrate $\xi_1, ..., \xi_6$ against the RCP scenarios, the DICE-2016 optimal scenario, and the historical spatial temperatures in 1900-2015 from the Goddard Institute for Space Studies (GISTEMP Team, 2018). For each scenario, we use its pathway of radiative forcing as the input F_t to our temperature system (4), which provides as output two regional pathways of atmospheric temperatures in the regions. Then we average the regional pathways to generate a globally averaged atmospheric temperature pathway. We calibrate a unique set of values for $\xi_1, ..., \xi_6$ so that the generated globally averaged atmospheric temperature pathways from our temperature system are close to the pathways of globally averaged atmospheric temperature for all scenarios and, at the same time, our regional temperatures in 2081-2100 are also close to the projected regional temperatures in 2081-2100 provided in IPCC (2013).

2.1.3 Sea Level Rise

Sea level rise is a serious problem caused by global warming. Table 4.1 of IPCC (2013) shows that, if the whole Greenland ice sheet melts, it will cause more than 7 meters (m) global mean SLR, and if the whole Antarctic ice sheet melts, it will lead to about 58 m global mean SLR. Moreover, once an ice sheet collapses, it is irreversible for millennia even if forcing is reversed

(IPCC 2013, Table 12.4). Nerem et al. (2018) adduce evidence that SLR is accelerating from the historical data. Table 13.5 of IPCC (2013) shows SLR in 2100 ranging from about 0.44 m for RCP2.6 to about 0.74 m for RCP8.5. Figure 13.14 of IPCC (2013) shows that the likely range of SLR is from 1 to 3 m per degree Celsius of globally averaged surface temperature increase if the warming is sustained for millennia.

There are four main sources of SLR: thermal expansion, and melting of glaciers and ice cap, the Greenland ice sheet, and the Antarctic ice sheet. The west Antarctic ice sheet (WAIS) is vulnerable to ocean warming as most of it is below sea level and extensively exposed to the ocean. The contribution of a complete collapse of the marine WAIS is estimated at 3.3 m of SLR (Bamber et al., 2009). Thermal expansion is also due to ocean warming. The melting of glaciers and the Greenland ice sheet is due to atmospheric warming in the North. Therefore, we assume that the rate of SLR is dependent on north atmospheric temperature $T_{t,1}^{\mathrm{TA}}$ and ocean temperature T_t^{OC}, and that a higher temperature implies a higher rate of SLR. We also assume that SLR, S_t, is irreversible. Thus, we let

$$S_{t+1} = S_t + \zeta_1^{\mathrm{SLR}} \left(T_{t,1}^{\mathrm{TA}}\right)^{\zeta_2^{\mathrm{SLR}}} + \zeta_3^{\mathrm{SLR}} T_t^{\mathrm{OC}}, \tag{5}$$

where ζ_1^{SLR}, ζ_2^{SLR} and ζ_3^{SLR} are calibrated using the SLR data for four RCP scenarios in Table 13.5 of IPCC (2013) and Table 1 of Kopp et al. (2014).

2.1.4 Permafrost Thaw

With global warming, and in particular with PA, a large amount of CO_2 and CH_4 could be emitted from thawing permafrost in the Arctic and sub-Arctic regions, which contain about 1,700 GtC (gigaton of carbon) in permafrost soils, while about 1,035 GtC are stored in the surface permafrost (0-3 m depth) and could easily be emitted when they are thawed (Schuur et al., 2015). Schuur et al. (2015) show that an average carbon release from the permafrost zone by 2100 across models is about 92 GtC with a standard deviation of 17 GtC under RCP8.5. A higher atmospheric temperature in the North implies a

higher emission rate. Thus, we assume that carbon emission from thawing permafrost is

$$E_t^{\text{Perm}} = \zeta_1^{\text{Perm}} \left(1 - \frac{1}{1 + \zeta_2^{\text{Perm}} T_{t,1}^{\text{AT}} + \zeta_3^{\text{Perm}} \left(T_{t,1}^{\text{AT}} \right)^2} \right). \tag{6}$$

Hope and Schaefer (2016) give a mean carbon emission path from thawing permafrost for the A1B scenario in IPCC (2007), so we use its annual time series[5] to calibrate ζ_1^{Perm}, ζ_2^{Perm} and ζ_3^{Perm}.

2.2 The Economic System

We calibrate our regional economic system to match RICE projections over our regions. Appendix A.3 shows that our calibrated system fits RICE projections.

2.2.1 Production

The gross output at time t in each region is determined by a Cobb-Douglas production function,

$$\mathcal{Y}_{t,i} \equiv A_{t,i} K_{t,i}^{\alpha} L_{t,i}^{1-\alpha}, \tag{7}$$

with $\alpha = 0.3$ and $L_{t,i}$ the exogenous population at time t and region i aggregated from RICE.[6]

We use region-specific total factor productivity (TFP) $A_{t,i}$. Sachs (2001) stresses ecological specific technical progress and lists five reasons why TFPs in low latitude zones tend to be smaller than temperate latitude zones. Of course there are exceptions, as Sachs points out (e.g., Hong Kong and Singapore and, now, lower latitude parts of China and parallel parts of "Asian Tigers"). However, theory suggests that the economies that are "behind" should grow faster than the leaders because the leaders have already done the "heavy lifting" of

[5]We thank Kevin Schaefer for providing the annual time series data.

[6]For region i and time t, we sum up population over the RICE subregions located in region i (if one RICE subregion is located across our border line 30°N, then we give a rough estimate with the ratio of land of the subregion located in the region i).

the TFP R&D which the followers could presumably copy. For example, Sachs and McArthur (2002) discuss the transition from "adopter" to "innovator" for countries.

We let

$$A_{t,i} = A_{0,i} \exp\left(\alpha_i^{\text{TFP}} \left(1 - \exp\left(-d_i^{\text{TFP}} t\right)\right) / d_i^{\text{TFP}}\right),$$

where $A_{0,i}$, α_i^{TFP} and d_i^{TFP} are calibrated to match the TFP path in region i which is computed from RICE by aggregating across the RICE subregions in region i.[7]

2.2.2 Damages

In the deterministic case of DIRESCU, we consider two types of damages: damages to output from SLR and damages to output directly from temperature increase.

We follow RICE to let

$$D_{t,i}^{\text{SLR}} = \pi_{1,i} S_t + \pi_{2,i} S_t^2 \tag{8}$$

reflect the damage from SLR, S_t, as a fraction of output. We calibrate $\pi_{1,i}$ and $\pi_{2,i}$ to match the damage from SLR which is computed from RICE.[8]

We follow DICE and RICE to assume a quadratic damage function for temperature increase

$$D_{t,i}^{\text{T}} = \pi_{3,i} T_{t,i}^{\text{AT}} + \pi_{4,i} (T_{t,i}^{\text{AT}})^2, \tag{9}$$

where $\pi_{3,i}$ and $\pi_{4,i}$ are calibrated to fit the aggregated projected damage from

[7] We first estimate $K_{t,i}$, $L_{t,i}$ and $\mathcal{Y}_{t,i}$ by summing over those in RICE subregions located in our region i for each time t, and then compute the TFP paths $A_{t,i} = \mathcal{Y}_{t,i}/(K_{t,i}^{\alpha} L_{t,i}^{1-\alpha})$ for region i.

[8] We estimate $\mathcal{Y}_{t,i}$ and $\mathcal{D}_{t,i}^{\text{SLR}} = D_{t,i}^{\text{SLR}} \mathcal{Y}_{t,i}$ by summing over those in RICE regions located in our region i for each time t, and then compute $D_{t,i}^{\text{SLR}} = \mathcal{D}_{t,i}^{\text{SLR}}/\mathcal{Y}_{t,i}$ for region i. With the data on the SLR path in RICE and $D_{t,i}^{\text{SLR}}$, we then calibrate $\pi_{1,i}$ and $\pi_{2,i}$ so that equation (8) holds approximately.

surface temperature change over RICE subregions.[9]

With the quadratic damage function (9) for the Tropic-South, this region has damage of only 9% of its output if its regional surface temperature increase is the same as the global mean surface temperature in 2100 under RCP8.5, i.e., 4.7°C, as RICE does not take into account catastrophic damages. However, Burke, Hsiang, and Miguel (2015) show that damages from high temperature increase in low- and mid-latitude regions are much higher, reducing projected global output by 23% in 2100 under RCP8.5, with the poorest 40% of countries (most being in our Tropic-South) having 75% reduction relative to a world without climate change. Dell, Jones, and Olken (2012) show that there are large and negative effects of higher temperatures on growth in poor countries, with about 1.3% economic growth reduction for a 1°C increase. Burke, Hsiang, and Miguel (2015) show that climate change may lead to negative economic growth for some countries. Our estimate of damages follows DICE and RICE, that is, damages are proportional to instantaneous output, not to growth of TFP, so they may be underestimated for the Tropic-South and overestimated for the North. However, our estimate of damages to the high-latitude regions may also be underestimated, as we ignored potential damages from inequality between the regions (Hsiang et al., 2017).

2.2.3 Emissions, Adaptation, and Mitigation

Global carbon emissions at time t are defined as

$$E_t \equiv \sum_{i=1}^{2} E_{t,i}^{\mathrm{Ind}} + E_t^{\mathrm{Perm}} + E_t^{\mathrm{Land}},$$

[9] We use the radiative forcing path in RICE to estimate $T_{t,i}^{\mathrm{AT}}$ using our calibrated climate equation (4). We also estimate $\mathcal{Y}_{t,i}$ and $\mathcal{D}_{t,i}^{\mathrm{T}} = D_{t,i}^{\mathrm{T}}\mathcal{Y}_{t,i}$ by summing over those in RICE regions located in our region i for each time t, and then compute $D_{t,i}^{\mathrm{T}} = \mathcal{D}_{t,i}^{\mathrm{T}}/\mathcal{Y}_{t,i}$ for region i. With the data on $T_{t,i}^{\mathrm{AT}}$ and $D_{t,i}^{\mathrm{T}}$, we then calibrate $\pi_{1,i}$ and $\pi_{2,i}$ so that equation (9) holds approximately.

where E_t^{Land} is exogenous global carbon emissions from biological processes, E_t^{Perm} is emissions from permafrost thawing estimated by equation (6), and

$$E_{t,i}^{\text{Ind}} = \sigma_{t,i}(1-\mu_{t,i})\mathcal{Y}_{t,i}$$

is industrial emissions, where $\mu_{t,i} \in [0,1]$ is an emission control rate and $\sigma_{t,i}$ is the carbon intensity in region i. We let

$$\sigma_{t,i} = \sigma_{0,i} \exp\left(-\alpha_i^\sigma \left(1-\exp\left(-d_i^\sigma t\right)\right)/d_i^\sigma\right), \tag{10}$$

where $\sigma_{0,i}$, α_i^σ and d_i^σ are calibrated to match the carbon intensity paths in region i which are computed from RICE by aggregating across the RICE sub-regions in region i.[10]

We include an adaptation choice variable $P_{t,i}$ for each region in our model as in de Bruin, Dellink, and Tol (2009). Adaptation reduces damages to output from SLR and temperature increase. In the deterministic case of DIRESCU, with adaptation the output net of climate damages becomes

$$Y_{t,i} \equiv \frac{\mathcal{Y}_{t,i}}{1+(1-P_{t,i})(D_{t,i}^{\text{SLR}} + D_{t,i}^{\text{T}})}, \tag{11}$$

where $P_{t,i} \in [0,1]$ is the adaptation rate. We follow de Bruin, Dellink, and Tol (2009) to assume that adaptation expenditure is

$$\Upsilon_{t,i} \equiv \eta_1 P_{t,i}^{\eta_2} Y_{t,i},$$

with $\eta_1 = 0.115$ and $\eta_2 = 3.6$.

We follow DICE to assume that mitigation expenditure is

$$\Psi_{t,i} \equiv \theta_{1,t,i}\mu_{t,i}^{\theta_2} Y_{t,i},$$

[10] We use the business-as-usual (BAU) results (i.e., with $\mu_{t,i} \equiv 0$) of RICE to estimate the carbon intensity paths. We first estimate $E_{t,i}^{\text{Ind}}$ and $\mathcal{Y}_{t,i}$ under BAU by summing over those in RICE subregions located in our region i for each time t, and then compute the carbon intensity paths $\sigma_{t,i} = E_{t,i}^{\text{Ind}}/\mathcal{Y}_{t,i}$ for region i.

where $\theta_{1,t,i}$ is the abatement cost as a fraction of output in region i at time t. We use the DICE/RICE form to define

$$\theta_{1,t,i} = b_{0,i} \exp\left(-\alpha_i^b t\right) \sigma_{t,i}/\theta_2,$$

where α_i^b and θ_2 are parameters given by RICE, and $b_{0,i}$ is the initial backstop price in region i.

Let $\widehat{Y}_{t,i}$ denote the output net of climate damage, mitigation expenditure and adaptation cost, that is,

$$\widehat{Y}_{t,i} = Y_{t,i} - \Psi_{t,i} - \Upsilon_{t,i}.$$

2.2.4 Economic Interactions between Regions

In the economic system, each region's stock of capital is the state variable $K_{t,i}$. Its law of motion is:

$$K_{t+1,i} = (1-\delta)K_{t,i} + I_{t,i}, \tag{12}$$

where $\delta = 0.1$ is the depreciation rate and $I_{t,i}$ is investment in region i. We model the economic interactions between two regions with the following adjustment cost function:

$$\Gamma_{t,i} \equiv \frac{B}{2}\widehat{Y}_{t,i}\left(\frac{I_{t,i} + c_{t,i}L_{t,i}}{\widehat{Y}_{t,i}} - 1\right)^2, \tag{13}$$

where B is the intensity of the friction, and $c_{t,i}$ is per capita consumption in region i. The open economy situation corresponds to $B = 0$, while a large B approximates the closed economy with $\widehat{Y}_{t,i} = I_{t,i} + c_{t,i}L_{t,i}$ (note that $\Gamma_{t,i} = 0$ could be caused by either the open economy or the closed economy, so we use $B = 0$ and large B to distinguish the two cases). Anderson and van Wincoop (2003) discuss border barriers and how costly they are. Similar adjustment cost functions have been used in Goulder, Hafstead, and Williams (2016). The economic interaction cost also includes the cost of avoiding carbon leakage between two regions. Eaton and Kortum (2002) find that if all countries (in

their data set) collectively remove tariffs, then most countries will gain around 1% of output with mobile labor, and less than 0.5% with immobile labor. Since we assume mobile labor within each region but immobile between two regions, we estimate the economic interaction cost to be roughly 0.5% of output for each region and use this to calibrate B.

The market clearing condition with adjustment costs becomes

$$\sum_{i=1}^{2} (I_{t,i} + c_{t,i}L_{t,i} + \Gamma_{t,i}) = \sum_{i=1}^{2} \widehat{Y}_{t,i}. \tag{14}$$

2.2.5 Social Welfare

In the deterministic case of the DIRESCU model, the total social welfare is defined as

$$\sum_{t=0}^{\infty} \beta^t \sum_{i=1}^{2} \tau_{t,i} u(c_{t,i}) L_{t,i},$$

where β is the discount factor, $\tau_{t,i}$ are weights for $i = 1, 2$, and u is a per capita utility function:

$$u(c) = \frac{c^{1-\frac{1}{\psi}}}{1-\frac{1}{\psi}}, \tag{15}$$

where ψ is the IES whose inverse is also the elasticity of marginal utility.

Therefore, the social planner's problem is

$$\max_{I_{t,i}, c_{t,i}, \mu_{t,i}, P_{t,i}} \quad \sum_{t=0}^{\infty} \beta^t \sum_{i=1}^{2} \tau_{t,i} u(c_{t,i}) L_{t,i}, \tag{16}$$

subject to transition laws (1), (4), (5), (12), and the market clearing constraint (14). The planner's problem has nine state variables: $K_{t,1}$, $K_{t,2}$, S_t, $\mathbf{M}_t$ (three-dimensional vector), and $\mathbf{T}_t$ (three-dimensional vector), as well as eight control variables $(I_{t,1}, I_{t,2}, c_{t,1}, c_{t,2}, \mu_{t,1}, \mu_{t,2}, P_{t,1}, P_{t,2})$ at each time t.

The egalitarian welfare criterion (i.e., $\tau_{t,i} \equiv 1$) and competitive welfare criterion (i.e., $\tau_{t,i}$ are Negishi weights) are employed to study the impact of either full cooperation or full competition between regions. However, in the

real world there exist both cooperation and competition at the same time (i.e., partial cooperation and partial competition), so we let

$$\tau_{t,i} = 1 + \lambda \left(\tau_{t,i}^{\text{Negishi}} - 1 \right),$$

where $\tau_{t,i}^{\text{Negishi}}$ are Negishi weights and the parameter $\lambda \in [0, 1]$ represents the level of competition between the regions. When $\lambda = 0$, it implies that there is no competition so it is a completely cooperative world ($\tau_{t,i} = 1$), while $\lambda = 1$ implies that this world is fully competitive ($\tau_{t,i} = \tau_{t,i}^{\text{Negishi}}$). We calibrate λ so that the consumption paths in each region of the model are close to the corresponding aggregated consumption paths in the RICE model. We compute Negishi weights by using an iterative numerical method with the following steps: (i) set the initial guess $\tau_{t,i}^{(0)} = 1$; (ii) for $k = 0, 1, 2, ...$, we solve model (16) with $\tau_{t,i}^{(k)}$ as the welfare weights to obtain the optimal per capita consumption paths $c_{t,i}^{(k)}$, and let

$$\tau_{t,i}^{(k+1)} = \frac{2 \left(u'(c_{t,i}^{(k)}) \right)^{-1}}{\sum_{j=1}^{2} \left(u'(c_{t,j}^{(k)}) \right)^{-1}};$$

and (iii) we stop the iteration if the difference between $\tau_{t,i}^{(k)}$ and $\tau_{t,i}^{(k+1)}$ is small for all t and i. In our examples, the stopping criterion is $\max_{t,i} \left| \tau_{t,i}^{(k+1)} - \tau_{t,i}^{(k)} \right| < 0.001$; we find that under this criterion, numerically the model has reached competitive equilibrium, which can be indicated by zero economic interaction and the same SCC between the regions obtained by the optimal solutions.

3 Results for the Deterministic Model

Since the choice of discount factor $\beta = 0.985$ means that welfare after 500 years has little impact on the solutions of the first 100 years, we approximate infinite-horizon problem (16) by an 800-year finite-horizon problem, assuming that: the last 300 years have fixed policy with $\mu_{t,i} \equiv 1$, $P_{t,i} \equiv P_{t,500}$; both

$c_{t,i}L_{t,i}/Y_{t,i}$ and $I_{t,i}/Y_{t,i}$ are constant; and $\Gamma_{t,i} = 0$ for $t \geq 501$. We then solve this finite-horizon optimal control problem with CONOPT in GAMS.

For the baseline deterministic model, we follow DICE-2016 to choose an IES of 0.69 and then calibrate λ to be 0.6. Figure 2 shows the optimal policy paths in this century. The top-left panel shows that the North always has a higher SCC than the Tropic-South. The initial SCC is \$53 per ton of carbon (/tC) for the North and \$42/tC for the Tropic-South, as the North is more developed and there exists partial cooperation between the two regions (the level of competition is $\lambda = 0.6$). However, the top-right panel shows a reverse direction for the adaption rate, implying that there are many more benefits from adaptation in the already hot Tropic-South, as the marginal damage as a fraction of regional output from 1℃ warming is much higher in the Tropic-South than in the North. The middle-left panel shows that the ratio of investment to regional output (i.e., $I_{t,i}/\widehat{Y}_{t,i}$) is lower in the North than in the Tropic-South, as the Tropic-South has larger TFP growth. The middle-right panel displays the PA pattern: the atmospheric temperature in the North reaches 5.2℃ at the end of this century, which is 2.3℃ higher than in the Tropic-South. Figure 2 clearly indicates that, under this simulation, the globally averaged surface temperature increase will be more than 3℃ in 2100, exceeding the 2℃ target set by the 2015 United Nations Climate Change Conference held in Paris. This temperature increase can be implied from the bottom-left panel showing that global industrial cumulative emissions in 2100 is 1000 GtC. The bottom-right panel shows that industrial emissions start to decline in the North after 2045, but continue growing in the Tropic-South and exceed those of the North after 2060. This is because most countries in the Tropic-South are developing and want to use cheaper fossil fuel to achieve faster economic growth. The baseline model indicates high industrial emissions because we follow the low-damage functions of DICE/RICE for the deterministic model.

To better identify the impacts of adaptation, SLR and permafrost thawing in the baseline deterministic model, we run it three times, leaving out one of them each time. We find that ignoring adaptation causes significant overestimation of the SCCs: the initial SCC is \$115/tC for the North and \$90/tC

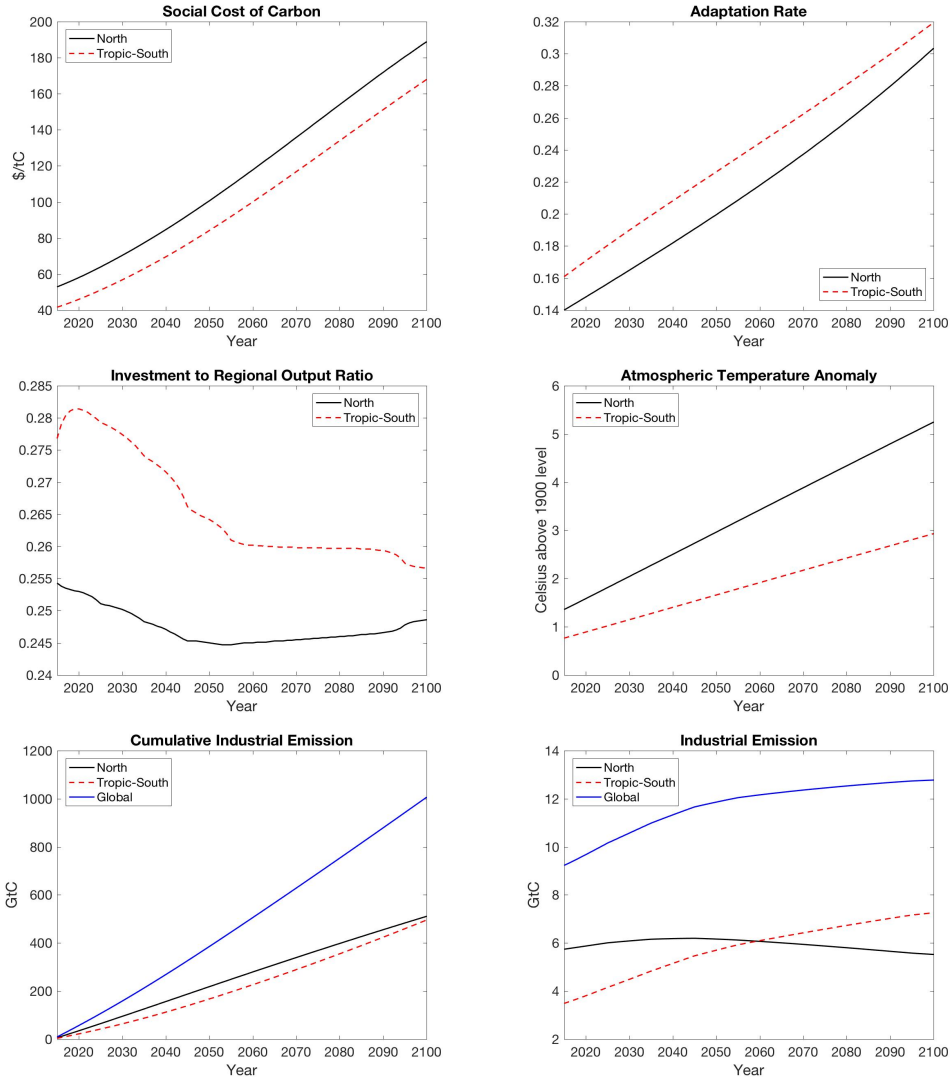

Figure 2: Optimal Policy for the Baseline Deterministic Model

for the Tropic-South, more than twice the corresponding initial SCCs with adaptation. In contrast, ignoring SLR causes significant underestimation of the SCCs: the initial SCC is \$32/tC for the North and \$26/tC for the Tropic-South, about 60% of the corresponding initial SCCs with SLR. We find that permafrost thawing has little impact on the SCCs: the initial SCC without permafrost thawing is only one dollar less than the initial SCC with permafrost thawing in each region. These results indicate that adaptation and SLR are important in IAMs and in calculation of the SCC, while permafrost thawing may not be.

3.1 Bias from Ignoring Heat Transport and PA

In order to take into account the PA effects in our model, we chose $\xi_4 = 0.6557$ and $\xi_5 = 0.5565$ as well as other related parameter values in the temperature subsystem. These parameters were chosen to match the data of the four RCP scenarios (after aggregation over the two regions), the DICE optimal scenario, the RICE optimal scenario (after aggregation over the RICE subregions for each of our regions), historical spatial data and predictive spatial data in IPCC (2013).

Figure 3 compares the optimal solutions using $\xi_4 = \xi_5 = 0$ (i.e., ignoring PA) to the solutions with PA. In the panels of Figure 3, the black and red lines represent solutions in the North and Tropic-South respectively. The solid lines show the default case with PA while the dashed lines show paths without PA. The top-left panel shows that the optimal SCC paths from ignoring heat transport are higher than those with heat transport for each region. By ignoring the heat and moisture transport, the paths of the North and Tropic-South atmospheric temperature anomaly merge after 2050 (top-right panel). The merged paths are between the temperature anomaly paths of the two regions with heat transport. That is, without the transport phenomena, we cannot detect PA in the model, and the temperature anomaly is underestimated in the North and overestimated in the Tropic-South. This implies that the solutions without heat transport will underestimate the damage in the North,

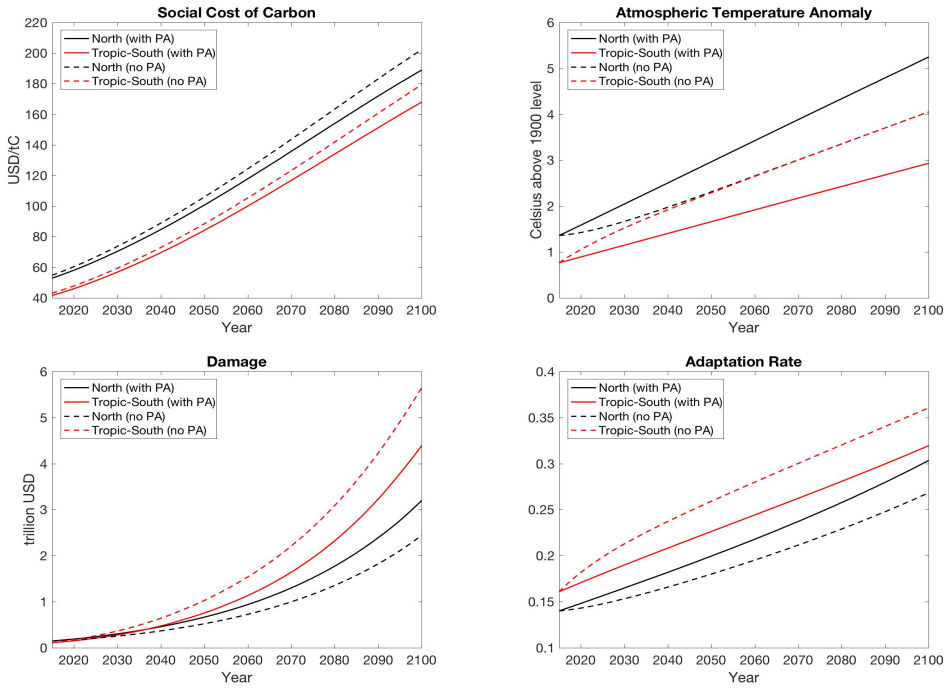

Figure 3: Bias of Optimal Solutions from Ignoring Heat Transport and PA

and overestimate it in the Tropic-South (bottom-left panel). The bias also exists in the optimal adaptation rates in the bottom-right panel: without heat transport, the adaptation rates in the North will be underestimated, as its corresponding atmospheric temperature anomaly is underestimated, and overestimated in the Tropic-South, as its corresponding atmospheric temperature anomaly is overestimated.

3.2 Sensitivity to Welfare Criteria

The baseline results are based on the model with partial cooperation between the two regions, with a competition level $\lambda = 0.6$. The literature usually just discusses two extreme cases: completely cooperative ($\lambda = 0$) and completely competitive ($\lambda = 1$). Figure 4 compares solutions of the SCC and economic interaction costs under three welfare criteria: partial cooperation with $\lambda = 0.6$; full cooperation with $\lambda = 0$; and no cooperation with $\lambda = 1$. Figure 4

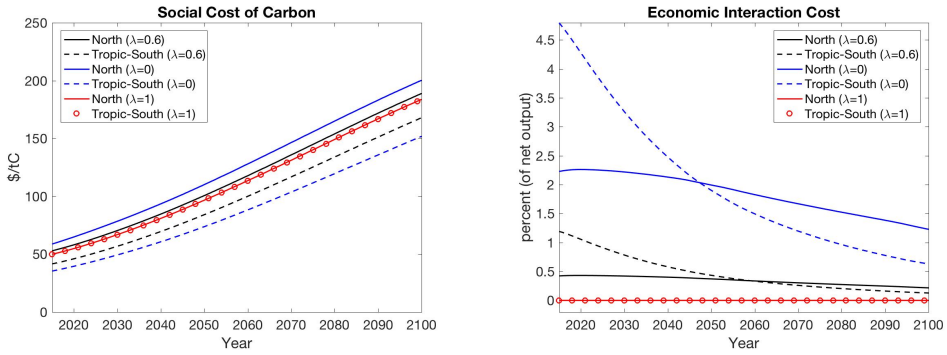

Figure 4: Solutions with Different Welfare Criteria

shows that, under full cooperation, the North has the highest SCC and the Tropic-South has the lowest SCC, while both regions have the highest economic interaction costs. This pattern appears because, under full cooperation, the more developed North would invest more in mitigation and also transfer more investment to the Tropic-South, in order to increase the total welfare of the world. Under no cooperation, both regions have the same SCC and zero economic interaction costs, as neither region would be willing to have more mitigation for the common good – the slowing down of global warming – and neither region would be willing to transfer any investment to the other region. Under partial cooperation, the results are between the two extreme cases.

3.3 Sensitivity to the IES

The above discussion assumes, following DICE-2016, that the IES (i.e., ψ) is equal to 0.69; however the value of the IES is debatable. For example, in the earlier versions of DICE (e.g., DICE-2007 (Nordhaus, 2008)), Nordhaus set the IES at 0.5. DSICE (Cai, Judd, and Lontzek, 2015) used a wide range of IESs from 0.5 to 2. In particular, for stochastic models, the IES is often larger than 1. This paper also discusses a case with $\psi = 1.5$. With different IESs, the model has different Negishi weights, so we recalibrate the level of competition at $\lambda = 0.4$ to match the per capita consumption growth under RICE. Figure 5 compares solutions of the deterministic model with different IESs ($\psi = 0.69$

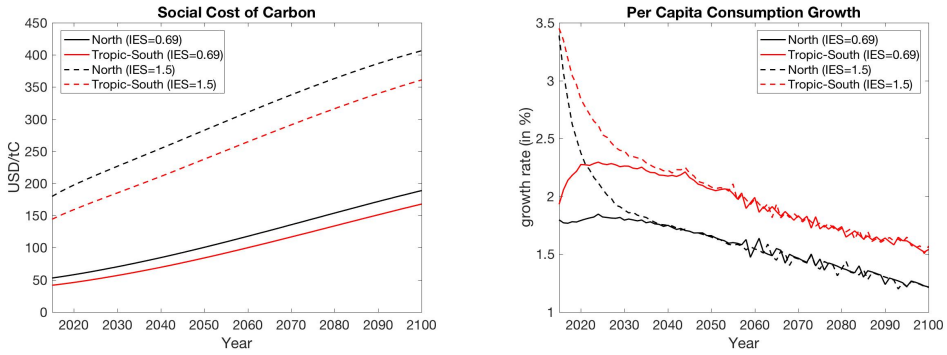

Figure 5: Solutions of the Deterministic Model with Different IES

with $\lambda = 0.6$, versus $\psi = 1.5$ with $\lambda = 0.4$). The left panel of Figure 5 shows that the higher IES leads to a higher SCC. For example, in the initial year, the SCC under $\psi = 1.5$ is about three times that of the SCC under $\psi = 0.69$ for each region. Under the higher IES, paths of per capita consumption growth (the right panel) are higher in the initial periods. The Tropic-South's growth under $\psi = 1.5$ is closer to the corresponding growth in RICE than it is under $\psi = 0.69$, but the reverse is true for the North's growth. However, under either $\psi = 0.69$ or $\psi = 1.5$, our model's growth paths are close to the RICE's growth path after 2040 in the North and the Tropic-South. The differences between the two cases are small for adaptation, economic interaction costs, damage and the atmospheric temperature (see Appendix A.4).

4 The Stochastic Model

There are many uncertainties in the economic and climate system. For example, DSICE (Cai, Judd, and Lontzek, 2015) discusses business cycle shocks in productivity and climate risks, and also deals with parameter uncertainty over the IES and risk aversion using uncertainty quantification. Lemoine and Traeger (2014) use a stylized model to study the impact of climate tipping points. Cai, Lenton, and Lontzek (2016) use DSICE to study the impact of multiple interacting tipping points on the carbon tax policy. In this paper we introduce uncertainty regarding the emergence of endogenous tipping elements

in the North into the spatial model with heat and moisture transport.

4.1 The Impact of Tipping Points

We assume that there is a representative tipping element that will take D years to fully unfold its damage after it occurs. The final damage level is $\overline{J}$ as a fraction of output, and the tipping probability depends on the contemporaneous atmospheric temperature in the North. Let J_t represent the damage level of the tipping element, and let χ_t be the indicator representing whether the tipping event has happened or not before time t, so $\chi_t = 0$ means that the tipping event has not happened, and $\chi_t = 1$ means that it has happened before time t. Thus, the transition law of J_t is

$$J_{t+1} = \min(\overline{J},\, J_t + \Delta)\chi_t, \tag{17}$$

where $\Delta = \overline{J}/D$ is the annual increment of damage level after the tipping happens, and χ_t is a Markov chain with the probability transition matrix

$$\begin{bmatrix} 1 - p_t & p_t \\ 0 & 1 \end{bmatrix},$$

where p_t is the tipping probability from state $\chi_t = 0$ to $\chi_t = 1$. We let

$$p_t = \exp\left(\varrho \max\left(0, T_{t,1}^{\mathrm{AT}} - 1\right)\right),$$

where ϱ is the hazard rate, so a higher atmospheric temperature in the North implies a higher tipping probability.

We use the Atlantic Meridional Overturning Circulation as the representative tipping element, and employ its default setup as in Cai, Lenton, and Lontzek (2016), that is, $D = 50$, $\overline{J} = 0.15$ and $\varrho = 0.00063$. To introduce a general model, we let

$$\chi_{t+1} = g(\chi_t, \mathbf{T}_t, \omega_t) \tag{18}$$

denote the transition law for χ_t. The output net of all damages including SLR,

temperature anomaly and tipping becomes

$$Y_{t,i} \equiv \frac{(1-J_t)\mathcal{Y}_{t,i}}{1+(1-P_{t,i})\left(D^{\mathrm{S}}_{t,i}+D^{\mathrm{T}}_{t,i}\right)}. \tag{19}$$

4.2 Recursive Preferences

We use Epstein–Zin (1989) preferences to isolate the IES and risk aversion for the stochastic model. With a transformation similar to that in Cai, Judd, and Lontzek (2015), we solve the Bellman equation:

$$V_t(\mathbf{x}_t) = \max_{\mathbf{a}_t} \sum_{i=1}^{2} \left\{ \tau_{t,i} u(c_{t,i}) L_{t,i} + \frac{\beta}{1-\frac{1}{\psi}} \left[\mathbb{E}_t \left(\left(\left(1-\frac{1}{\psi}\right) V_{t+1}(\mathbf{x}_{t+1}) \right)^{\Theta} \right) \right]^{1/\Theta} \right\}, \tag{20}$$

subject to (1), (4), (5), (12), (14), (17), (18) and (19), where

$$\mathbf{x}_t = (K_{t,1}, K_{t,2}, M^{\mathrm{AT}}_t, M^{\mathrm{UO}}_t, M^{\mathrm{DO}}_t, T^{\mathrm{AT}}_{t,1}, T^{\mathrm{AT}}_{t,2}, T^{\mathrm{OC}}_t, S_t, J_t, \chi_t)$$

is the vector of state variables (ten continuous variables and one binary variable), $\mathbf{a}_t = (I_{t,1}, I_{t,2}, c_{t,1}, c_{t,2}, \mu_{t,1}, \mu_{t,2}, P_{t,1}, P_{t,2})$ is the vector of decision variables (all are continuous), $\mathbb{E}_t$ is the expectation operator conditional on the time-t information, and $\Theta = (1-\gamma)/(1-1/\psi)$ where ψ is the IES and γ is the risk aversion parameter. We use annual time steps, where the initial year ($t = 0$) is 2015, and the terminal time ($t = T = 500$) is the year 2515. The terminal value function $V_T(\mathbf{x}_T)$ is computed as shown in Appendix A.5. When there is no risk, equation (20) is equivalent to the deterministic model (16).

We use $\psi = 1.5$ and $\gamma = 3.066$ as in Pindyck and Wang (2013) as well as $\tau_{t,i} = 1 + \lambda\left(\tau^{\text{Negishi}}_{t,i} - 1\right)$ with $\lambda = 0.4$ for our benchmark stochastic case, where $\tau^{\text{Negishi}}_{t,i}$ are the Negishi weights for the deterministic model with $\psi = 1.5$.

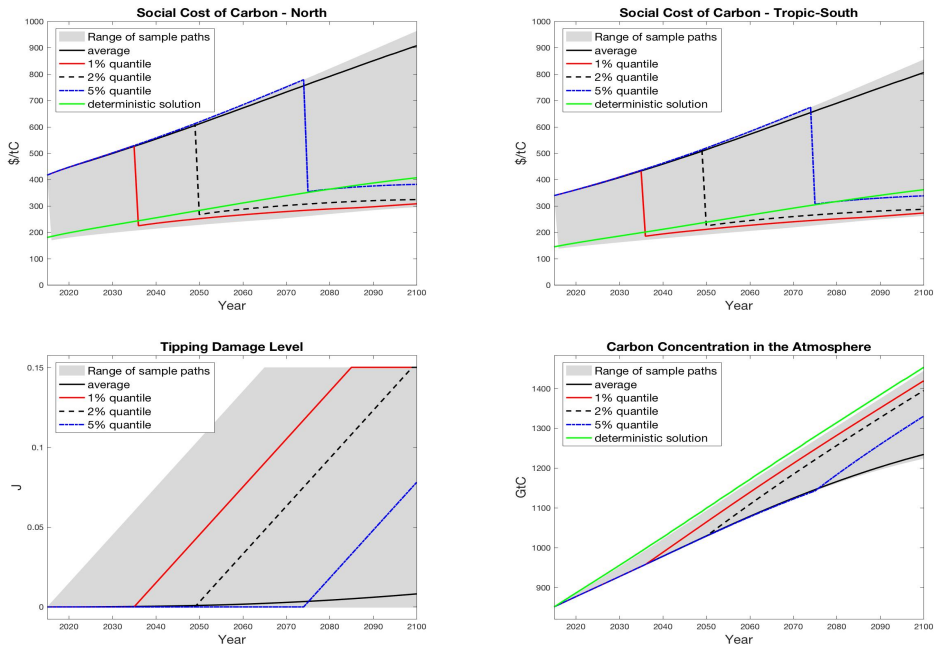

Figure 6: Optimal SCC, Tipping Damage Level, and Atmospheric Carbon for the Stochastic Model

5 Results from the Stochastic Model

We solve the Bellman equation (20) using parallel dynamic programming (Cai, Judd, and Lontzek, 2015) via backward induction on the Blue Waters supercomputer. After we solve the Bellman equation, we use the optimal policy functions to generate 10,000 simulation paths forward. That is, each simulation path starts at the observed initial states, we simulate one sample of the shock for the tipping point at time t, and then with the realized sample and the optimal control policy at t, we obtain the optimal states at $t+1$.

The two top panels of Figure 6 show the distributions of the simulated optimal SCC for both regions. All the panels in Figure 6, as well as in Figure 7, include a line representing the deterministic case derived with the same IES used in the stochastic model. The shaded area represents the range of the 10,000 sample paths, along with the average, 1%, 2% and 5% quantile paths (that is, at each point in time, we compute the average and these quantiles of

10,000 values). The initial SCC increases significantly from the deterministic case to the stochastic case, as the initial SCC for the stochastic case is \$416/tC for the North and \$339/tC for the Tropic-South, about 2.3 times that of the corresponding deterministic case (with $\psi = 1.5$ and $\lambda = 0.4$) in each region. The cumulative probability that the tipping event will occur before 2100 is only 9.5%, while the 1%, 2% and 5% cumulative probability of tipping occurs in years 2035, 2050, and 2074 respectively. Once the tipping event happens, the SCC immediately falls significantly, but damages unfold over a 50-year period, as shown in the bottom-left panel for the tipping damage level J_t. This happens because the high SCC before tipping is intended to prevent or delay the tipping point as its occurrence depends on the contemporaneous temperature. However, after the tipping event happens, this incentive disappears as the damage will unfold in a deterministic way. This result is consistent with the finding in DSICE. The bottom-right panel shows that, with the stricter mitigation policy, the stochastic model has smaller carbon concentration in the atmosphere and in 2100 it is on average 200 GtC less than the corresponding deterministic simulation (with $\psi = 1.5$ and $\lambda = 0.4$). If the tipping event occurs, then the carbon concentration has a higher rate of increase as the corresponding mitigation policy is less strict.

Figure 7 shows the distributions of the optimal simulation paths for atmospheric temperatures and adaptation rates in both regions for the stochastic model. By comparing the two top panels, we see that the North has a much higher temperature anomaly than the Tropic-South for the stochastic solutions. Moreover, the atmospheric temperature anomaly in the North is about 2℃ higher than in the Tropic-South in 2100. The two bottom panels show the optimal adaptation rates. Again we see that the North has lower adaptation rates than the Tropic-South for the stochastic solutions, and that the stochastic results have lower adaptation rates than the corresponding deterministic case, since with the stricter mitigation policy and the resulting lower temperatures in the stochastic case, there is less need to adapt.

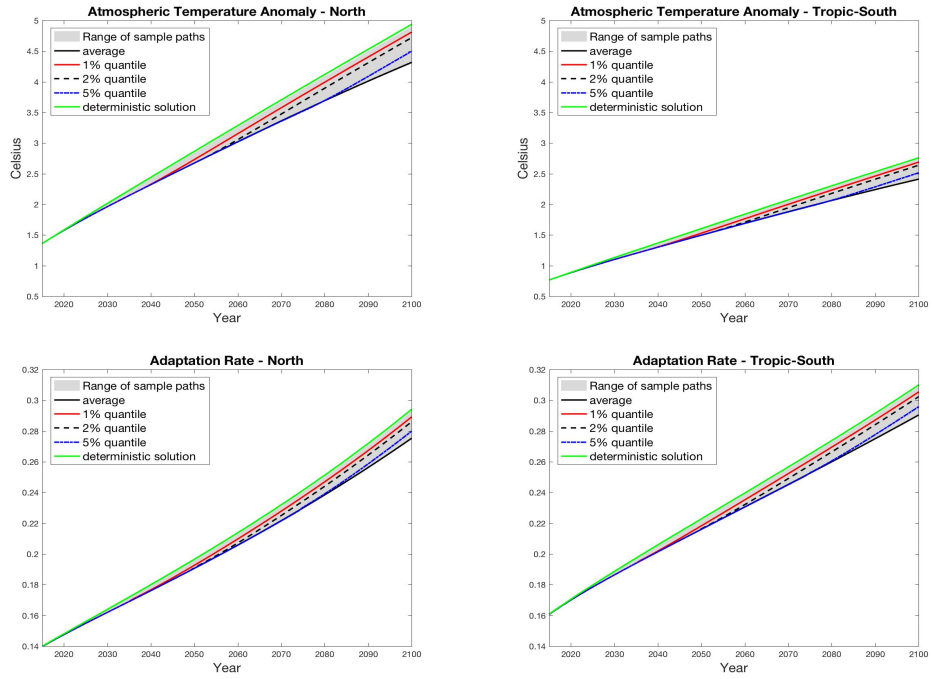

Figure 7: Temperature and Adaptation Rate for the Stochastic Model

5.1 Bias from Ignoring Heat Transport and PA

We examine the bias from ignoring heat and moisture transport and PA (i.e., $\xi_4 = \xi_5 = 0$) again for the stochastic case, shown in Figure 8. In each panel of the figure, the black lines represent the average paths and the red lines represent the 1% quantile paths. The solid lines show the case with heat and moisture transport and PA, while the dashed lines show the case without it.

The top panels of Figure 8 show that ignoring heat transport and PA underestimates the SCCs for both regions in the early periods. For example, the initial SCC with $\xi_4 = \xi_5 = 0$ is about 10% less than in the case with PA for both regions. Note that this is in the opposite direction to the deterministic case shown in the top-left panel of Figure 3, where ignoring heat transport overestimates the SCC. This is because ignoring heat transport leads to a lower temperature in the North (see bottom-left panel of Figure 8) and then underestimates the tipping probability which depends on the atmospheric temperature in the North. This is also reflected in the 1% quantile paths: the

case ignoring PA has a 1% cumulative probability of tipping in year 2044, nine years later than in the case with PA. This lower tipping probability means a less risky tipping element which leads to smaller SCCs. The middle and bottom panels of Figure 8 show that ignoring heat transport and PA significantly underestimates the atmospheric temperature anomaly and adaptation rates in the North, and significantly overestimates them in the Tropic-South.

5.2 Sensitivity on the IES, Risk Aversion and Welfare Criterion

As shown in Section 3, results depend on values of the IES and the welfare criterion. For the stochastic model, they also depend on risk aversion. Different values of risk aversion are used in the literature (e.g., $\gamma = 3.066$ in Pindyck and Wang (2013) and $\gamma = 10$ in Bansal and Yaron (2004) and Cai, Judd, and Lontzek (2015)). Table 1 lists the initial SCC for various IESs ($\psi \in \{0.69, 1.5\}$), welfare criterion according to the level of competition ($\lambda \in \{0, 0.4, 0.6, 1\}$) and risk aversion ($\gamma \in \{3.066, 10\}$). Note that the stochastic model with $\lambda = 1$ is just an approximation of real competitive equilibrium, so the initial SCC of the North is not equal to that of the Tropic-South for the stochastic cases, but they are still close to each other for every case (with $\lambda = 1$). Moreover, when $\lambda = 1$, the simulated SCC paths in the North are close to those in the Tropic-South, and the simulated economic interaction costs (in ratios of regional output) are close to zero. These imply that the Negishi weights from the deterministic model (i.e., $\lambda = 1$) are appropriate for approximating the competitive equilibrium in the stochastic cases in this paper.

Table 1 shows that a higher IES leads to a higher SCC in both regions; that a higher risk aversion leads to a higher SCC in both regions; and that stochastic cases have a higher SCC than deterministic cases for the same IES and λ. This finding is consistent with Cai, Judd, and Lontzek (2015). Table 1 also shows that a higher level of competition leads to a smaller SCC in the North and a larger SCC in the Tropic-South. Moreover, Table 1 shows that the

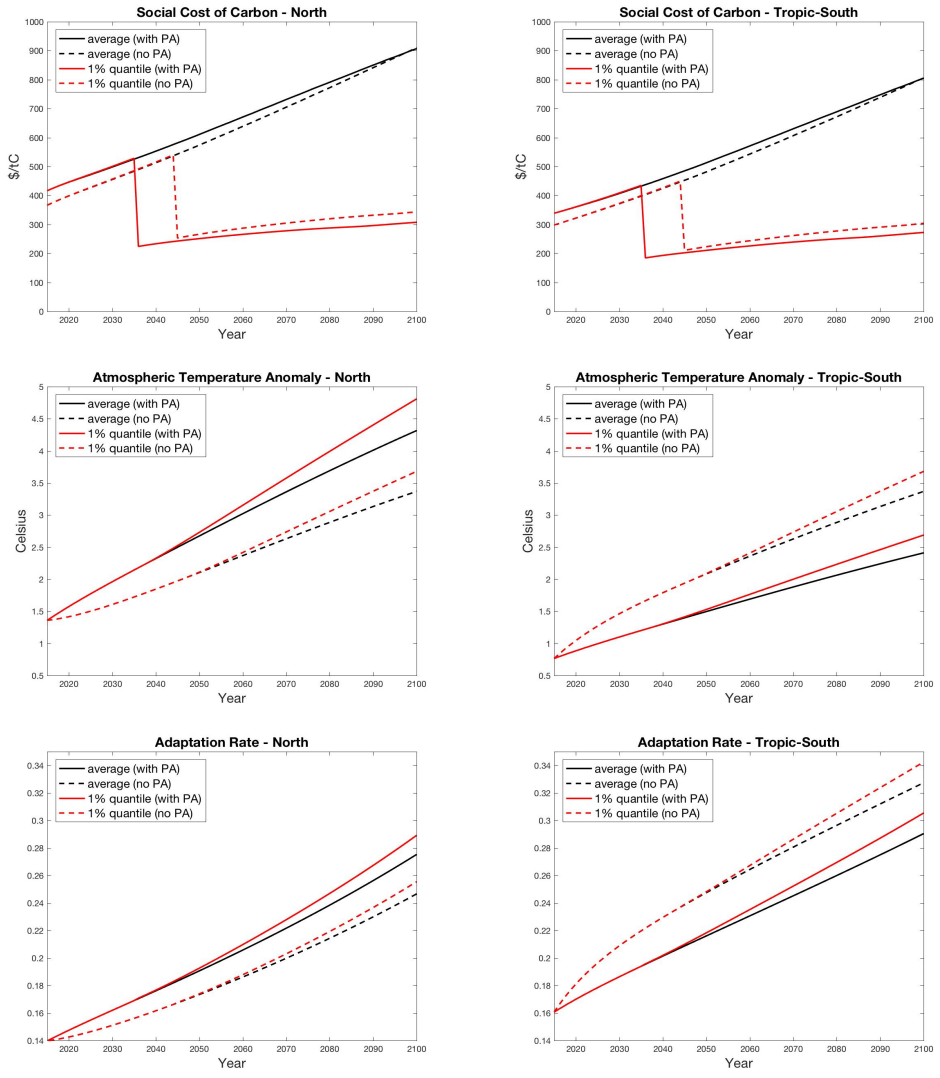

Figure 8: Bias of Solutions from Ignoring Heat Transport and PA for the Stochastic Model

Table 1: Initial SCC under various IESs (ψ), welfare criterion (level of competition λ), and risk aversion (γ)

IES (ψ)	λ	Deterministic		Stochastic			
		North	Tropic -South	North		Tropic-South	
				$\gamma = 3.066$	$\gamma = 10$	$\gamma = 3.066$	$\gamma = 10$
0.69	0	59	35	111	130	68	79
	0.4	55	39	104	121	75	88
	0.6	53	42	101	118	81	94
	1	50	50	96	112	97	114
1.5	0	193	135	446	510	316	361
	0.4	180	144	416	477	339	387
	0.6	174	150	403	460	352	402
	1	163	163	378	431	384	438

North has a higher SCC than the Tropic-South for all cases, except that the North has a slightly smaller SCC than the Tropic-South for the stochastic cases with $\lambda = 1$ due to approximation errors for the competitive equilibrium. This finding is consistent with our findings for the deterministic model in Section 3.

6 Conclusion

This paper has taken a first step toward adding a heretofore neglected element – dynamic heat and moisture transport from the lower latitudes toward the Poles – into computational IAMs used in policy-relevant climate economics. We divided the world into the North and the Tropic-South where the North is the region from 30°N latitude to the North Pole and the Tropic-South is the rest of the world. Our temperature anomaly dynamics for the North and the Tropic-South has two key positive parameters (ξ_4, ξ_5) which were calibrated using historical and projection data. The impact of neglecting heat and moisture transport on the optimal paths of key quantities – temperature, the SCC, emissions, adaptation and damages – can be assessed in our model by setting $\xi_4 = \xi_5 = 0$ and observing how the optimal paths change.

When our model is calibrated to data, we find substantial biases in key

quantities such as temperature anomalies, adaptation rates, the SCC and damages, relative to the case where a social planner neglects poleward heat and moisture transport. We also show how potential arrival times of tipping elements in the high latitudes are affected by the transport phenomena and, most importantly, how these tipping elements can affect the SCC between the two regions.

As indicated in Sections 3.1 and 5.1 (and Figures 3 and 8), the biases from neglecting heat and moisture transport are quite substantial. Note that in this paper we have abstracted from the nonlinearity caused by surface albedo feedback which is likely to add even larger effects than what we see in Figure 3 because its effects are in the same direction.

In this paper the directional heat and moisture transport from regions closer to the Equator toward regions closer to the Poles is combined, in the same model, with endogenous SLR, permafrost thawing, stochastic arrival of tipping points, cooperation and different levels of competition between the North and Tropic-South, and recursive preferences which distinguish between risk aversion and the IES. We believe that these aspects of our model constitute an important step forward in calibrated IAMs at the "coarse grained" level of aggregation, which can improve the development of scientifically-informed and scientifically-disciplined climate change policies.

We expect that future research and extensions in the context of our model – which would involve a finer regional disaggregation, nonlinear surface albedo feedbacks, and better approximations of damages from sources such as SLR, permafrost thawing or tipping points – could provide additional and improved insights.

References

Anderson, James E. and Eric van Wincoop. 2003. "Gravity with Gravitas: A Solution to the Border Puzzle." *American Economic Review* 93 (1):170–192.

Bamber, Jonathan L., Riccardo E. M. Riva, Bert L. A. Vermeersen, and

Anne M. LeBrocq. 2009. "Reassessment of the Potential Sea-Level Rise from a Collapse of the West Antarctic Ice Sheet." *Science* 324 (5929):901–903.

Bansal, Ravi, Dana Kiku, and Marcelo Ochoa. 2016. "Price of Long-Run Temperature Shifts in Capital Markets." Working Paper 22529, National Bureau of Economic Research.

Bansal, Ravi and Amir Yaron. 2004. "Risks for the Long Run: A Potential Resolution of Asset Pricing Puzzles." *The Journal of Finance* 59 (4):1481–1509.

Barreca, Alan, Karen Clay, Olivier Deschenes, Michael Greenstone, and Joseph S. Shapiro. 2016. "Adapting to Climate Change: The Remarkable Decline in the US Temperature-Mortality Relationship over the Twentieth Century." *Journal of Political Economy* 124 (1):105–159.

Bekryaev, Roman V., Igor V. Polyakov, and Vladimir A. Alexeev. 2010. "Role of polar amplification in long-term surface air temperature variations and modern Arctic warming." *Journal of Climate* 23:3888–3906.

Brock, W. and A. Xepapadeas. 2017. "Climate change policy under polar amplification." *European Economic Review* 94:263–282.

Burgess, Robin, Olivier Deschenes, Dave Donaldson, and Michael Greenstone. 2014. "The unequal effects of weather and climate change: Evidence from mortality in india." Working paper.

Burke, Marshall, Solomon M. Hsiang, and Edward Miguel. 2015. "Global non-linear effect of temperature on economic production." *Nature* 527 (7577):235–239.

Cai, Yongyang, Kenneth L. Judd, and Thomas S. Lontzek. 2015. "The social cost of carbon with economic and climate risks." Working paper, arxiv:1504.06909.

Cai, Yongyang, Timothy M. Lenton, and Thomas S. Lontzek. 2016. "Risk of multiple interacting tipping points should encourage rapid CO2 emission reduction." *Nature Climate Change* 6 (5):520–525.

Cohen, Judah, Karl Pfeiffer, and Jennifer A. Francis. 2018. "Warm Arctic episodes linked with increased frequency of extreme winter weather in the United States." *Nature Communications* 9 (1):869.

de Bruin, Kelly C., Rob B. Dellink, and Richard S. J. Tol. 2009. "AD-DICE: an implementation of adaptation in the DICE model." *Climatic Change* 95 (1):63–81.

Dell, Melissa, Benjamin F. Jones, and Benjamin A. Olken. 2012. "Temperature Shocks and Economic Growth: Evidence from the Last Half Century." *American Economic Journal: Macroeconomics* 4 (3):66–95.

Eaton, Jonathan and Samuel Kortum. 2002. "Technology, Geography, and Trade." *Econometrica* 70 (5):1741–1779.

Epstein, Larry G. and Stanley E. Zin. 1989. "Substitution, Risk Aversion, and the Temporal Behavior of Consumption and Asset Returns: A Theoretical Framework." *Econometrica* 57 (4):937–969.

GISTEMP Team. 2018. "GISS Surface Temperature Analysis (GISTEMP). NASA Goddard Institute for Space Studies." URL `https://data.giss.nasa.gov/gistemp/`. Accessed on March 7, 2018.

Golosov, Mikhail, John Hassler, Per Krusell, and Aleh Tsyvinski. 2014. "Optimal Taxes on Fossil Fuel in General Equilibrium." *Econometrica* 82 (1):41–88.

Goulder, Lawrence H., Marc A. C. Hafstead, and III Williams, Roberton C. 2016. "General Equilibrium Impacts of a Federal Clean Energy Standard." *American Economic Journal: Economic Policy* 8 (2):186–218.

Hassler, John and Per Krusell. 2012. "Economics and climate change: integrated assessment in a multi-region world." *Journal of the European Economic Association* 10 (5):974–1000.

Hope, Chris and Kevin Schaefer. 2016. "Economic impacts of carbon dioxide and methane released from thawing permafrost." *Nature Climate Change* 6 (1):56–59.

Hsiang, Solomon, Robert Kopp, Amir Jina, James Rising, Michael Delgado, Shashank Mohan, D. J. Rasmussen, Robert Muir-Wood, Paul Wilson, Michael Oppenheimer, Kate Larsen, and Trevor Houser. 2017. "Estimating economic damage from climate change in the United States." *Science* 356 (6345):1362–1369.

IPCC. 2007. *Climate Change 2007, The Physical Science Basis*. New York: Cambridge University Press.

———. 2013. *Climate Change 2013, The Physical Science Basis*. New York: Cambridge University Press.

Kopp, Robert E., Radley M. Horton, Christopher M. Little, Jerry X. Mitrovica, Michael Oppenheimer, D. J. Rasmussen, Benjamin H. Strauss, and Claudia Tebaldi. 2014. "Probabilistic 21st and 22nd century sea-level projections at a global network of tide-gauge sites." *Earth's Future* 2 (8):383–406.

Krusell, Per and Anthony Smith. 2017. "Climate Change Around the World." memo.

Langen, Peter L. and Vladimir A. Alexeev. 2007. "Polar amplification as a preferred response in an idealized aquaplanet GCM." *Climate Dynamics* 29 (2):305–317.

Lemoine, Derek and Christian Traeger. 2014. "Watch Your Step: Optimal Policy in a Tipping Climate." *American Economic Journal: Economic Policy* 6 (1):137–166.

Lenton, Timothy M. and Hans Joachim Schellnhuber. 2007. "Tipping the scales." *Nature Reports Climate Change* 1:97–98.

Meinshausen, M., S.C.B. Raper, and T.M.L. Wigley. 2011. "Emulating coupled atmosphere-ocean and carbon cycle models with a simpler model, MAGICC6: Part I - Model Description and Calibration." *Atmospheric Chemistry and Physics* 11:1417–1452.

Meinshausen, M., S.J. Smith, K. Calvin, J.S. Daniel, M.L.T. Kainuma, J-F. Lamarque, K. Matsumoto, S.A. Montzka, S.C.B. Raper, K. Riahi, A. Thomson, G.J.M. Velders, and D.P.P. van Vuuren. 2011. "The RCP greenhouse gas concentrations and their extensions from 1765 to 2300." *Climatic Change* 109:213–241.

Negishi, T. 1972. *General equilibrium theory and international trade.* Amsterdam: North-Holland Publishing Company.

Nerem, R. S., B. D. Beckley, J. T. Fasullo, B. D. Hamlington, D. Masters, and G. T. Mitchum. 2018. "Climate-change–driven accelerated sea-level rise detected in the altimeter era." *Proceedings of the National Academy of Sciences* .

Nordhaus, William D. 2008. *A Question of Balance: Weighing the Options on Global Warming Policies.* Yale University Press.

———. 2010. "Economic aspects of global warming in a post-Copenhagen environment." *Proceedings of the National Academy of Sciences* 107 (26):11721–11726.

———. 2017. "Revisiting the social cost of carbon." *Proceedings of the National Academy of Sciences of the United States of America* 114 (7):1518–1523.

Overland, James E. and Muyin Wang. 2018. "Arctic-midlatitude weather linkages in North America." *Polar Science* URL `https://www.sciencedirect.com/science/article/pii/S1873965217301160`.

Pindyck, Robert S. and Neng Wang. 2013. "The Economic and Policy Consequences of Catastrophes." *American Economic Journal: Economic Policy* 5 (4):306–339.

Sachs, Jeffrey D. 2001. "Tropical Underdevelopment." Working Paper 8119, National Bureau of Economic Research.

Sachs, Jeffrey D. and John W. McArthur. 2002. "Technology and the New Economy." chap. Technological Advancement and Long-term Economic Growth in Asia. Cambridge, MA, USA: MIT Press, 157–185.

Schuur, E. A. G., A. D. McGuire, C. Schadel, G. Grosse, J. W. Harden, D. J. Hayes, G. Hugelius, C. D. Koven, P. Kuhry, D. M. Lawrence, S. M. Natali, D. Olefeldt, V. E. Romanovsky, K. Schaefer, M. R. Turetsky, C. C. Treat, and J. E. Vonk. 2015. "Climate change and the permafrost carbon feedback." *Nature* 520 (7546):171–179.

van der Ploeg, Frederick and Aart de Zeeuw. 2016. "Non-cooperative and Cooperative Responses to Climate Catastrophes in the Global Economy: A North-South Perspective." *Environmental and Resource Economics* 65 (3):519–540.

Appendices For Online Publication

A.1 Definition of Parameters and Exogenous Paths

In DIRESCU, we approximate the exogenous paths of DICE-2016 in five-year time steps by their annual analogs. The land carbon emissions E_t^{Land} and exogenous radiative forcing F_t^{EX} are defined below:

$$E_t^{\text{Land}} = 0.95e^{-0.115t} \tag{A.1}$$

$$F_t^{\text{EX}} = \begin{cases} 0.5 + 0.00588t, & \text{if } t \leq 85 \\ 1, & \text{otherwise.} \end{cases} \tag{A.2}$$

Tables A.1-A.3 list the values and/or definition of all parameters, variables and symbols.

Table A.1: Parameters, Variables and Symbols in the Deterministic Climate System

t	time in years ($t = 0$ represents year 2015)
$i \in \{1, 2\}$	region i (North or Tropic-South)
M_t^{AT}	carbon concentration in the atmosphere (billion tons); $M_0^{\mathrm{AT}} = 851$
M_t^{UO}	carbon concentration in upper ocean (billion tons); $M_0^{\mathrm{UO}} = 460$
M_t^{DO}	carbon concentration in deep ocean (billion tons); $M_0^{\mathrm{DO}} = 1740$
$\mathbf{M}_t = \left(M_t^{\mathrm{AT}}, M_t^{\mathrm{UO}}, M_t^{\mathrm{DO}}\right)^\top$	carbon concentration vector
$T_{t,i}^{\mathrm{AT}}$	average surface temperature (Celsius); $T_{0,1}^{\mathrm{AT}} = 1.36$, $T_{0,2}^{\mathrm{AT}} = 0.765$
T_t^{OC}	average ocean temperature (Celsius); $T_0^{\mathrm{OC}} = 0.0068$
$\mathbf{T}_t = \left(T_{t,1}^{\mathrm{AT}}, T_{t,2}^{\mathrm{AT}}, T_t^{\mathrm{OC}}\right)^\top$	temperature vector
S_t	sea level rise (SLR); $S_0 = 0.14$
F_t	global radiative forcing
F_t^{EX}	exogenous radiative forcing
$\eta = 3.68$	radiative forcing parameter
Φ_{M}	transition matrix of carbon cycle
$\mathbf{\Phi}_{\mathrm{T}}$	transition matrix of temperature system
$\phi_{1,2} = 0.0237$, $\phi_{2,1} = 0.0388$	parameters in transition matrix of carbon cycle
$\phi_{2,3} = 0.00136$, $\phi_{3,2} = 0.00284$	parameters in transition matrix of carbon cycle
$\xi_1 = 0.0526$, $\xi_2 = 0.08987$	parameters in transition matrix of temperature system
$\xi_3 = 0.0022$, $\xi_4 = 0.6557$	parameters in transition matrix of temperature system
$\xi_5 = 0.5565$, $\xi_6 = 0.0$	parameters in transition matrix of temperature system
$\zeta_1^{\mathrm{SLR}} = 0.00073$, $\zeta_2^{\mathrm{SLR}} = 1.4$	parameters in SLR by warming
$\zeta_3^{\mathrm{SLR}} = 0.007$	parameters in SLR by warming
$\zeta_1^{\mathrm{Perm}} = 1.951$, $\zeta_2^{\mathrm{Perm}} = -0.0858$	parameters in emission from permafrost thawing by warming
$\zeta_3^{\mathrm{Perm}} = 0.2257$	parameters in emission from permafrost thawing by warming
$M_*^{\mathrm{AT}} = 588$	equilibrium atmospheric carbon concentration

Table A.2: Parameters, Variables and Symbols in the Economic System

$\mathcal{Y}_{t,i}$	gross output
$Y_{t,i}$	output net of damage
$\widehat{Y}_{t,i}$	output net of damage, abatement and adaptation cost
$A_{t,i}$	total productivity factor (TFP); $A_{0,1} = 7.331$, $A_{0,2} = 3.582$
$\alpha_1^{\text{TFP}} = 0.013$, $\alpha_2^{\text{TFP}} = 0.0184$	initial growth of TFP
$d_1^{\text{TFP}} = 0.0053$, $d_2^{\text{TFP}} = 0.0061$	change rate of growth of TFP
$L_{t,i}$	population (in billions)
$K_{t,i}$	capital (in \$ trillions); $K_{0,1} = 146$, $K_{0,2} = 77$
$\alpha = 0.3$	output elasticity of capital
$D_{t,i}^{\text{S}}$	damage (in fraction of output) from sea level rise
$\pi_{1,1} = 0.00447$, $\pi_{1,2} = 0.00408$	SLR damage parameter
$\pi_{2,1} = 0.01146$, $\pi_{2,2} = 0.00646$	SLR damage parameter
$D_{t,i}^{\text{T}}$	damage (in fraction of output) from surface temperature anomaly
$\pi_{3,1} = 0.00094$, $\pi_{3,2} = 0.00322$	non-SLR damage parameter
$\pi_{4,1} = 0.0002$, $\pi_{2,2} = 0.00074$	non-SLR damage parameter
$\Psi_{t,i}$	mitigation expenditure
$\Upsilon_{t,i}$	adaptation expenditure
$\mu_{t,i}$	emission control rate
E_t, $E_{t,i}^{\text{Ind}}$, E_t^{Land}	global emission; regional industrial emission; land emission
$P_{t,i}$	adaptation rate
$\sigma_{t,i}$	carbon intensity; $\sigma_{0,1} = 0.094$, $\sigma_{0,2} = 0.104$
$\alpha_1^\sigma = 0.0156$, $\alpha_2^\sigma = 0.0181$	initial declining rate of carbon intensity
$d_1^\sigma = 0.0063$, $d_2^\sigma = 0.007$	change rate of growth of carbon intensity
$\theta_2 = 2.6$	mitigation cost parameter
$\theta_{1,t,i}$	adjusted cost for backstop
$b_{0,1} = 1.71$, $b_{0,2} = 2.19$	initial backstop price
$\alpha_1^b = \alpha_2^b = 0.005$	declining rate of backstop price
$\eta_1 = 0.115$, $\eta_2 = 3.6$	parameters for adaptation cost
$\delta = 0.1$	annual depreciation rate
$c_{t,i}$	per capita consumption
$I_{t,i}$	investment
$\Gamma_{t,i}$	adjustment cost for economic interaction between regions
$B = 1$	parameter for economic interaction cost
$\psi \in \{0.69, 1.5\}$	IES
u	per capita utility function
$\tau_{t,i}$	weights
λ	level of competition between two regions
$\beta = 0.985$	discount factor

Table A.3: Additional Parameters, Variables and Symbols in the Stochastic Model

$D = 50$	duration of tipping process
J_t	damage level; $J_0 = 0$
$\overline{J} = 0.15$	final damage level
Δ	annual increment of damage level
$\chi_t \in \{0, 1\}$	indicator for whether tipping has happened; $\chi_0 = 0$
p_t	tipping probability
$\varrho = 0.00063$	hazard rate for tipping
$\gamma \in \{3.066, 10\}$	risk aversion parameter
$\mathbf{x}_t$	vector of state variables
V_t	value function

A.2 Calibration of the Climate System

Figure A.1 shows that our calibrated carbon cycle can approximate well for all scenarios except RCP8.5. Since RCP8.5 is the business-as-usual scenario, and our model is solving problems with optimal mitigation policy, the deviation of approximation for RCP8.5 has little impact on our solutions.

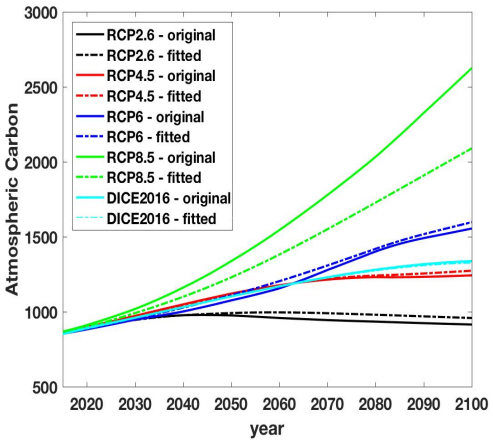

Figure A.1: Fitting Atmospheric Carbon Concentration

Figure A.2 shows that our calibrated temperature system can approximate well for all these scenarios. Figure A.3 displays the corresponding spatial sur-

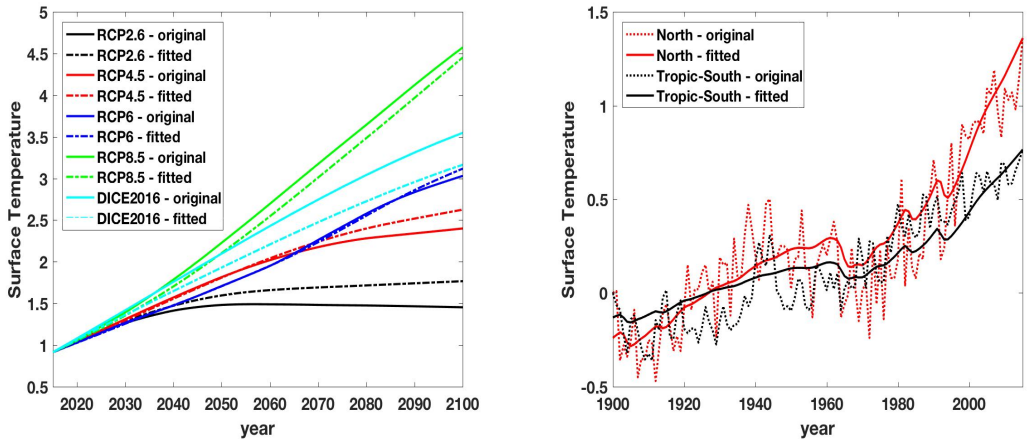

Figure A.2: Fitting Surface Temperature

face temperature and ocean temperature pathways from the calibrated temperature system, for the RCP scenarios and the DICE-2016 optimal scenario. It also shows that the spatial surface temperatures in 2081-2100 are close to the ones given in IPCC (2013).

Figure A.4 shows that our fitted paths of SLR (above the level in 2000) for RCP2.6, RCP4.5 and RCP6 are quite close to the mean projections in IPCC (2013) and Kopp et al. (2014).

The left panel of Figure A.5 shows that our function (6) for estimating emissions from thawing permafrost fits data well, and the right panel of Figure A.5 shows projected future cumulative emission paths from thawing permafrost since 2010 for four RCP scenarios. We see that the cumulative carbon emission under RCP8.5 is also inside the likely range given in Schuur et al. (2015).[11]

[11]Since the amount of GHGs in permafrost is finite, we can have an upper bound constraint on cumulative emissions from permafrost. But since our model solution never hits the upper bound, numerically this constraint does not matter.

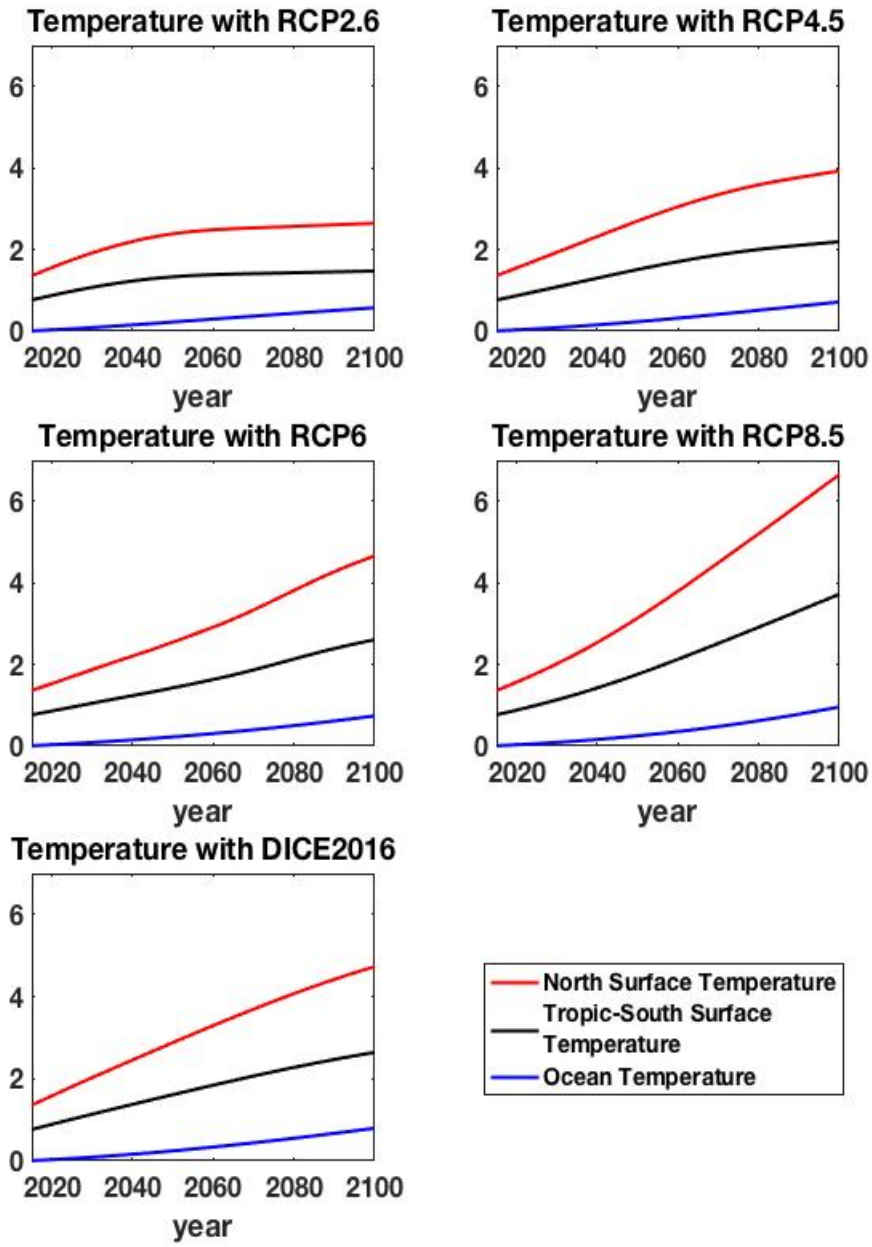

Figure A.3: Spatial Temperature Using RCP or DICE Radiative Forcing Scenarios

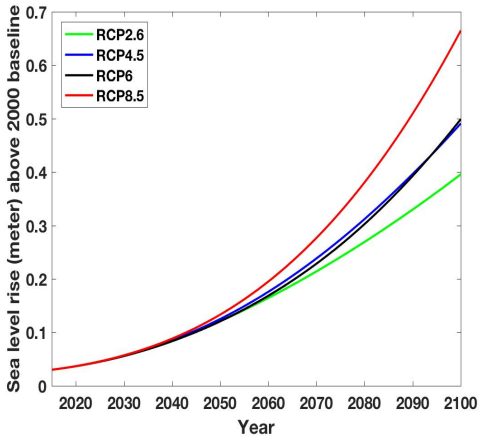

Figure A.4: Fitting SLR

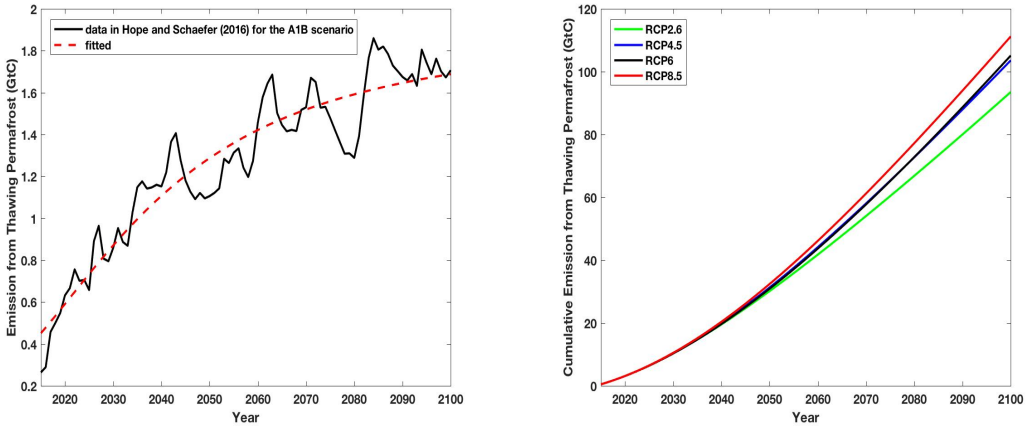

Figure A.5: Fitting the Carbon Emission Data from Thawing Permafrost and Projecting Future Cumulative Emission Paths from Thawing Permafrost since 2010

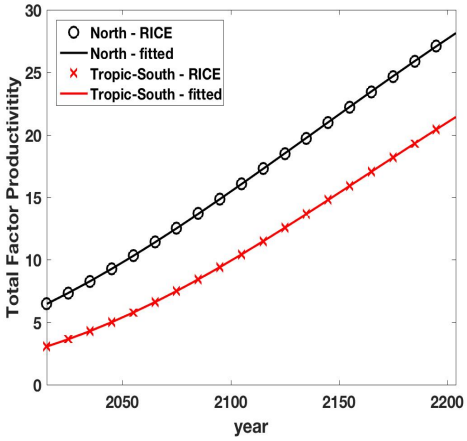

Figure A.6: Fitting Total Factor Productivity

A.3 Calibration of the Economic System

Figure A.6 shows that our calibrated TFP paths match RICE projections over both the North and the Tropic-South.

Figure A.7 shows that our estimate of SLR damage function (8) is close to the RICE projection of SLR damage for both the North and the Tropic-South.

Figure A.8 shows that our non-SLR damage functions (9) fit the RICE projection of non-SLR damage in fraction of output.

Figure A.9 shows that our carbon intensity estimate (10) closely approximates the corresponding RICE projections.

A.4 Supplementary Results

Figure A.10 shows the optimal emission control rate paths and SLR for the baseline deterministic case. The left panel shows that the North has higher emission control rates than the Tropic-South. The right panel shows that SLR increases at an increasing rate over time and reaches about 0.69 m (above the pre-indsutrial level) in 2100. This happens because in the simulation the surface and ocean temperatures continue to rise in this century, and therefore ice sheets (e.g., Greenland ice sheet and Antarctic ice sheet) melt at higher

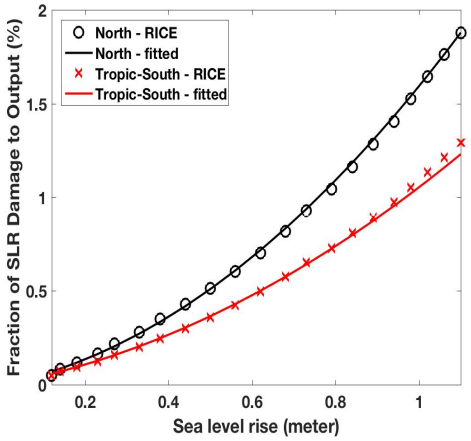

Figure A.7: Fitting SLR Damage to Output

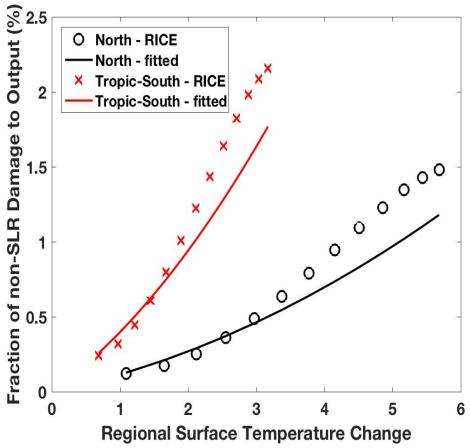

Figure A.8: Fitting Non-SLR Damage to Output

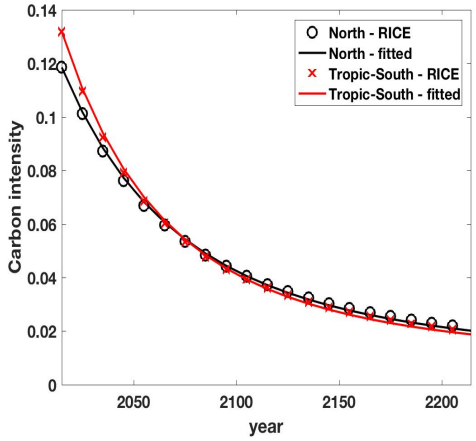

Figure A.9: Fitting Carbon Intensity

rates.

The left panel of Figure A.11 shows that, for the baseline deterministic case ($\psi = 0.69$ and $\lambda = 0.6$), per capita consumption growth in the Tropic-South starts at around 2% in the initial year and ends at 1.5% at the end of this century, while the North has lower growth, starting at 1.8% and ending at 1.2% in 2100. The difference between the two growth paths is caused by the spillover effect of technology from the North to the Tropic-South. The economic interaction cost between the two regions for the baseline deterministic case is shown in the right panel of Figure A.11: both regions have declining economic interaction cost in ratios to regional output, while the North declines from 0.42% in the initial year to 0.21% in 2100, and the Tropic-South starts at 1.2% and drops to 0.14% in 2100.

Figure A.12 shows that, for the baseline deterministic case, changes in the IES have little impact on optimal adaptation, economic interaction cost, damages and atmospheric temperature.

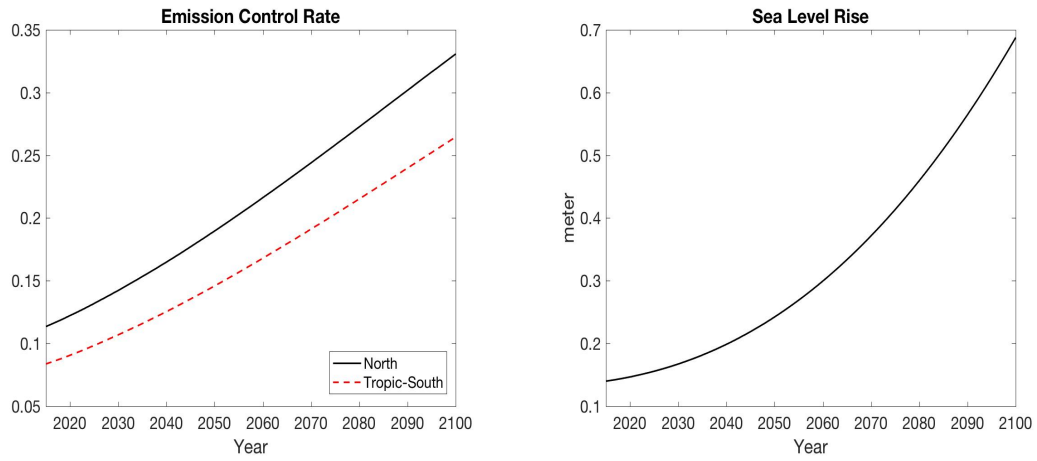

Figure A.10: Solutions in the Climate System of the Deterministic Model

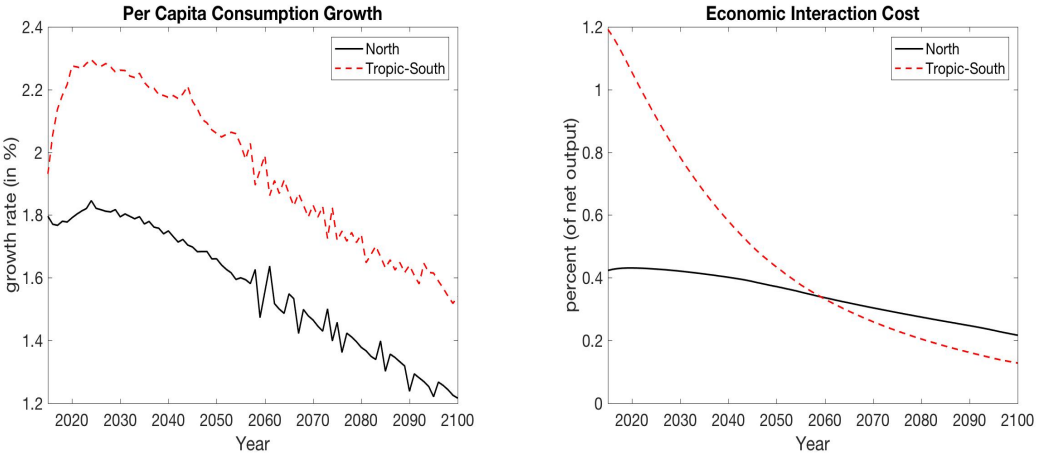

Figure A.11: Solutions in the Economic System of the Deterministic Model

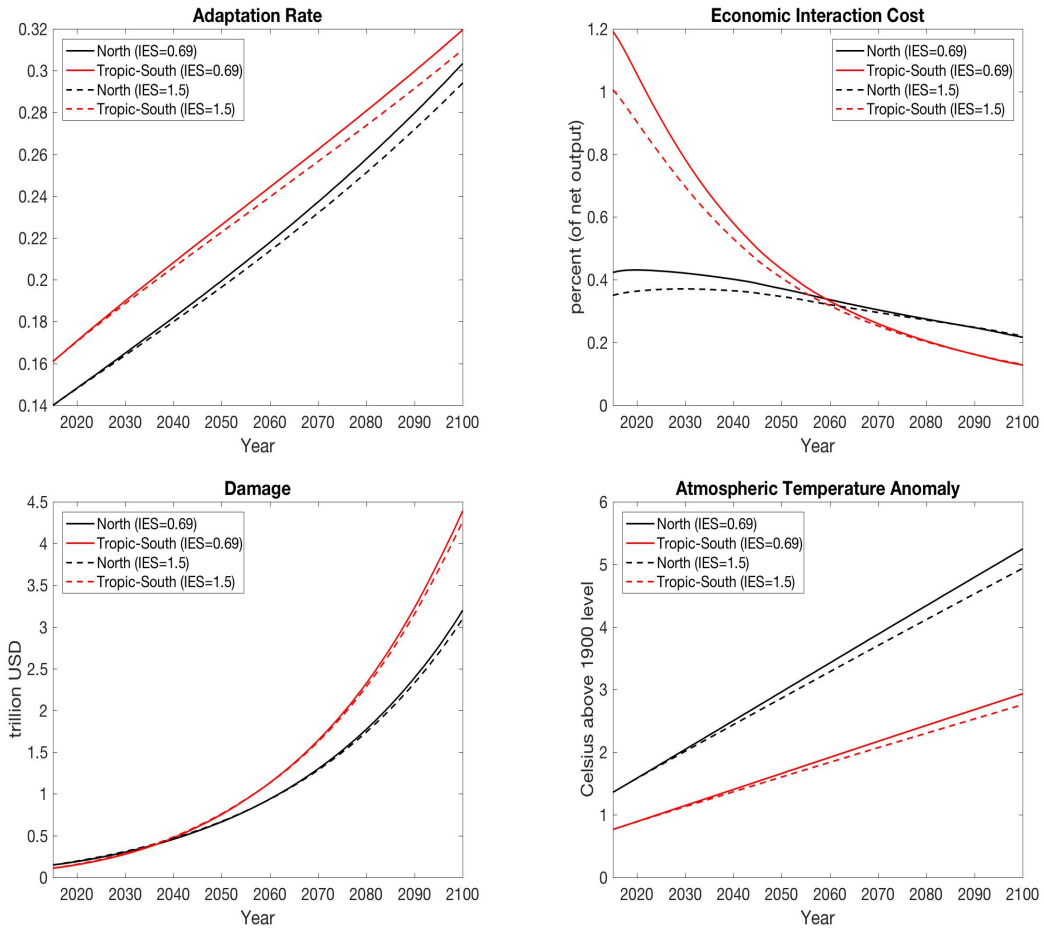

Figure A.12: Comparison between Solutions of the Deterministic Model with Different IESs

A.5 Terminal Value Function

The terminal value function at terminal time $T = 500$ is computed as

$$V_T(\mathbf{x}_T) = \tau_{T,i} L_{T,i} \sum_{t=500}^{800} \beta^{t-500} u(c_{t,i}),$$

where we assume that for all $t > T$, all exogenous paths stop changing and fix their values at terminal time T. Emission control rates are always 1 (i.e., $\mu_{t,i} = 1$), adaptation rates are fixed at the optimal levels of the deterministic model at the terminal time, there are no economic interaction costs (i.e., $\Gamma_{t,i} = 0$), both $c_{t,i} L_{t,i} / Y_{t,i}$ and $I_{t,i} / Y_{t,i}$ are given constant values and, if the tipping event has not happened before T, then it never happens; or if the tipping event has happened, then its damage will unfold until its maximum level.